ASME Journal of Offshore Mechanics and Arctic Engineering
Online journal at:
https://asmedigitalcollection.asme.org/offshoremechanics

Computational Investigation of Scour Around Square Piles Oriented at 45 deg and 90 deg in Wave–Current Flows

Lalit Kumar
Department of Maritime and Transport Technology,
Faculty of Mechanical Engineering,
Delft University of Technology,
Delft 2628, The Netherlands
e-mail: L.Kumar-1@tudelft.nl

Mohammad Saud Afzal[1]
Department of Civil Engineering,
Indian Institute of Technology Kharagpur,
Kharagpur, West Bengal 721302, India
e-mail: saud@civil.iitkgp.ac.in

Said Alhaddad
Department of Maritime and Transport Technology,
Faculty of Mechanical Engineering,
Delft University of Technology,
Delft 2628, The Netherlands
e-mail: S.M.S.Alhaddad@tudelft.nl

Square piles are widely utilized in coastal engineering due to their economic efficiency and robustness in resisting large forces in the coastal environment. However, the removal of sediment particles due to the approaching flow around such structures, known as scour, raises concerns about the stability and safety of the structure. Therefore, this study investigates scour around square piles placed at 45 deg and 90 deg angles in wave–current flows. A newly developed sediment transport module within the open-source REEF3D framework is developed, incorporating a three-phase semicoupled approach with level-set method (LSM) for realistic representation of sediment bed and free surface interfaces. The developed model is first validated against experimental results of circular and square pile scour in different flow conditions, such as steady current, wave-only, and wave–current flows. Furthermore, the effect of the combined wave–current parameter (U_{cw}) and Keulegan–Carpenter (KC) number on the normalized equilibrium scour depth (S/D_w) is explored. This study provides new insights into how square pile orientation modifies bed topography and equilibrium scour depth in wave–current flows. Numerical results demonstrate that a higher S/D_w value was observed for larger U_{cw} and KC numbers for both piles. It is revealed that in wave-only and combined wave–current flows with low KC numbers ($KC < 10$), square piles oriented at 45 deg experience greater scour depths than those oriented at 90 deg. However, at a higher KC number ($KC = 18$), square piles oriented at 90 deg exhibit greater scour depths compared to those at 45 deg.
[DOI: 10.1115/1.4070801]

Keywords: square pile, scour, horseshoe vortex, vortex shedding, combined wave–current flows, coastal engineering, computational fluid dynamics

1 Introduction

Piles have emerged as famous coastal and marine structures due to their excellent structural stability and exceptional load-bearing capacity. Nonetheless, the introduction of piles in a wave–current condition complicates the flow physics and scour phenomenon in coastal environments [1,2]. Pile-induced turbulence results in the formation of a turbid wake [3], which may lead to environmental repercussions [4]. The scour phenomenon substantially threatens the safety and reliability of such expensive coastal structures. Besides, excessive scour can cause geotechnical instabilities, such as breaching, which takes place when a slope larger than the angle of repose is formed [5–7].

Therefore, it is crucial to examine the scour phenomena around the pile in wave–current flows. Most studies on pile scour were conducted under steady current or wave-only cases [8–18]. A limited number of studies focused on pile scour in a combined wave–current environment [19–24]. In steady currents, the formation of scour around a pile is mainly governed by the horseshoe vortex (HSV), downflow, lee-wake vortices, and streamline contraction [25–27]. However, HSV and shedding of vortex are the main factors governing the development of scour holes around the pile in the wave-only condition [28,29]. In this case, scour is primarily affected by two dimensionless factors: (1) Keulegan–Carpenter (KC) number and (2) diffraction parameter for large piles (D_w/L, where D_w is the pile width obstructing the flow and L is the wavelength) [30]. The KC number represents the distance a water particle travels during one wave cycle relative to the pile width. A higher KC value indicates that the water motion is more extensive, corresponding to stronger or longer-duration waves, whereas a lower KC value reflects weaker or shorter waves with limited particle movement. The nondimensional KC number is expressed as given in Eq. (1).

$$\mathrm{KC} = \frac{U_w T}{D_w} \tag{1}$$

where U_w is the wave orbital velocity, and T is the wave period.

[1]Corresponding author.

Contributed by the Ocean, Offshore, and Arctic Engineering Division of ASME for publication in the Journal of Offshore Mechanics and Arctic Engineering. Manuscript received August 15, 2025; final manuscript received December 28, 2025; published online January 30, 2026. Assoc. Editor: Masoud Hayatdavoodi.

In oscillatory flows, the HSV plays a critical role in scour formation around piles for KC ≤ 100 [28]. However, a less effect of HSV on scour was reported for KC numbers ranging from 6 to 30 [31]. Sumer et al. [29] conducted experiments to investigate wave-induced scour around 45 deg and 90 deg oriented square piles. They observed that vortex shedding is absent for a 45 deg oriented square pile when the KC number is less than 4, and for a 90 deg oriented square pile when the KC number is less than 11. They also reported that square piles oriented at 45 deg experienced a higher equilibrium scour depth when compared to square piles oriented at 90 deg in the wave-only condition.

The combination of waves and currents complicates the flow hydrodynamics that involves nonlinear interactions between waves and current rather than simply adding the linear components of steady current and waves [30]. Soulsby and Whitehouse [32] reported that wave–current interactions lead to (1) increased bed shear stress components due to the interaction of the waves and the current's boundary layer, (2) the development of wave-induced currents, and (3) wave refraction caused by currents altering the wavelength and phase speed of the waves. Umeyama [33–35] also conducted experimental investigations to examine flow hydrodynamics under a combined wave–current environment. Their research mainly focused on analyzing the turbulent characteristics and free surface interface under varying wave–current parameters (U_{cw}), calculated as given in Eq. (2). The U_{cw} parameter quantifies the relative strength of the steady current compared to the maximum oscillatory wave velocity near the bed. The higher U_{cw} values indicate a flow dominated by the current, whereas lower values correspond to conditions primarily governed by wave motion.

$$U_{cw} = \frac{U_c}{U_c + U_w} \tag{2}$$

where U_c is the current velocity at a vertical distance $y = D/2$ from the seabed.

Sumer and Fredsøe [23] conducted experiments to examine the scour around a circular pile in the wave–current environment. They reported that the introduction of current to the oscillatory flow causes a larger pile scour depth for KC numbers less than 100. The dominance of the current component on scour depth formation was observed when U_{cw} was equal to or greater than 0.7. These conclusions were derived from experiments conducted with irregular waves propagating co-directionally or orthogonally to the current. Furthermore, Qi and Gao [21,22] examined the effect of wave-generated pore pressure on monopile scour in wave–current flows (opposing and co-directional). Qi and Gao [22] also reported the effect of the average-velocity-based Froude number (Fr_a) on circular pile scour. They additionally suggested an empirical equation to calculate the equilibrium scour depth using Fr_a in wave–current flows, as represented in Eq. (3).

$$\begin{aligned} \lg(S/D_w) = &-0.80\exp(0.14/\mathrm{Fr}_a) \\ &+ 1.11\ (0.1 < \mathrm{Fr}_a < 1.1,\ 0.4 < KC < 26) \end{aligned} \tag{3}$$

where $Fr_a = U_a/(gD_w)^{0.5}$, g is the gravitational acceleration, and U_a is the average water particle velocity in wave–current flows, which can be calculated using Eq. (4).

$$U_a = \left[\frac{1}{T/4}\int_0^{T/4}(U_c + U_w \sin(2\Pi t/T))dt = U_c + \frac{2}{\Pi}U_w\right] \tag{4}$$

Using physical experiments, Chen and Li [19] examined the circular pile scour in the wave–current condition. They reported that the nonlinearity of waves can result in the migration of scour downstream. This phenomenon is attributed to the irregularities in the crests and troughs of the waves. Recently, Schendel et al. [36] examined the monopile scour in waves combined with oblique currents. They observed that the equilibrium scour depths decreased as the wave spreading increased, suggesting a greater influence of KC numbers. Several numerical investigations are also performed on pile scour in the wave–current condition [37–41]. Afzal et al. [10] utilized the REEF3D model to conduct a numerical investigation on pile scour in wave–current flows. They employed the level-set method (LSM) in their simulations to represent free surface interfaces and established a favorable correlation between the simulated outcomes and experimental observations. Gautam et al. [39] utilized the REEF3D numerical model to examine the influence of KC number on equilibrium scour depth around circular piles for different U_{cw} values. They found that the normalized equilibrium scour depth (S/D_w) becomes larger with an increased KC number for a given value of U_{cw}.

Although several studies have investigated local scour around circular piles under steady current, wave-only, and combined wave–current flows [19,21,23,39], research on noncircular pile geometries, particularly square piles, remains limited. Existing experimental investigations on square piles have mainly focused on wave-only conditions [29], with few addressing the effects of combined wave–current interactions or pile orientation. However, the influence of square pile orientation (45 deg and 90 deg) on equilibrium scour depth, temporal development of scour, and bed morphology under combined wave–current flow is still not well understood. Furthermore, the combined influence of the KC number and U_{cw} parameter on scour evolution around square piles has not been systematically quantified.

To address these research gaps, the present study performs a comprehensive three-dimensional numerical investigation of scour around square piles under combined wave–current flows. The newly developed sediment transport module in the REEF3D framework [42–48] is employed using a three-phase (air–water–sediment) semicoupled formulation with the LSM to capture free surface and bed evolution accurately. The present study systematically examines the effects of square pile orientation (45 deg and 90 deg), KC number ($3.9 < KC < 18$), and U_{cw} parameter on scour evolution and introduces new correlations between the normalized equilibrium scour depth (S/D_w) and the average-velocity-based Froude number (Fr_a). The findings provide novel numerical insights into the influence of pile geometry and flow interaction parameters on scour processes, therefore advancing current understanding and offering practical guidance for the design and safety assessment of coastal and offshore foundations.

2 Numerical Model

The open-source code REEF3D (Release 23.01) is used to study the scour around square piles with 45 deg and 90 deg orientations in the combined wave–current condition. The employed computational fluid dynamics (CFD) model is a three-phase semicoupled model incorporating the air, water, and sediment phases [42,48]. An advantage of the numerical model is its utilization of the LSM, which realistically represents the sediment bed and free surface interface [47].

2.1 Hydrodynamic Modeling. REEF3D simulates 3D flow hydrodynamics using the incompressible Reynolds-averaged Navier–Stokes (RANS) equations for momentum conservation and the continuity equation for mass conservation, as shown in Eqs. (5) and (6).

$$\frac{\partial U_i}{\partial x_i} = 0 \tag{5}$$

$$\frac{\partial U_i}{\partial t} + U_j\frac{\partial U_j}{\partial x_j} = -\frac{1}{\rho}\frac{\partial P}{\partial x_i} + \frac{\partial}{\partial x_j}\left[(\nu + \nu_t)\left(\frac{\partial U_i}{\partial x_j} + \frac{\partial U_j}{\partial x_i}\right)\right] + g_i \tag{6}$$

where ρ is the fluid mass density, U is the time average velocity over time t, P is the pressure, ν is the kinematic viscosity, and ν_t is the turbulent eddy viscosity.

The fifth-order weighted essentially non-oscillatory (WENO) scheme is used to discretize the advection and diffusion components of the RANS equations [49]. The turbulence and free surface variables are handled using the Hamilton–Jacobi version of the WENO scheme [50]. To simulate the pressure, Chorin's projection technique [51] is used. To prevent odd-even decoupling between pressures and velocities, a staggered grid is used. Time discretization is accomplished using the third-order total variation diminishing Runge–Kutta technique [52]. An adaptive time-stepping technique is used to optimize the time-step size. An adaptive time stepping is implemented throughout the simulations to ensure the accuracy and stability of the numerical model. The size of the time-step is determined based on the Courant–Friedrichs–Lewy number, as reported by Griebel et al. [53]. For the hydrodynamic turbulence computation, the k–ω model [54] is employed, as discussed in detail by Gautam et al. [39]. The time coupling between the hydrodynamic and sediment transport solvers was achieved through REEF3D's standard temporal-decoupling approach [43]. The hydrodynamic solver was advanced with a time-step of $\Delta t = 0.001$ s, while the sediment transport and bed-update calculations were executed every 10 hydrodynamic time steps, corresponding to a morphological acceleration factor of 10 ($\Delta t_m = 0.01$ s). This approach ensures numerical stability and computational efficiency while accurately reproducing the equilibrium scour depths observed in the simulations.

2.2 Sediment Transport Modeling. The sediment transport phenomenon plays a crucial role in the erosion and deposition of sediments. There are two primary methods through which the sediment particle is transported: bedload and suspended load transport. These modes are differentiated based on the relationship between critical bed shear stress and settling velocity [55].

Shields approach [56] is used to compute the incipient motion of sediment grains, in which the critical bed shear stress is computed using the critical Shields parameter. Furthermore, the turbulent viscosity equation (7) is utilized to calculate the effective bed stresses.

$$\tau = -\rho(\nu_t + \nu)\frac{\partial u}{\partial z} \tag{7}$$

where z represents the depth from the zero bed level.

At the onset of scouring, alterations in both longitudinal and transverse bed slopes trigger changes in bed topography. Consequently, the consideration of sloping beds becomes imperative in determining the critical bed shear stress (τ_0), as it governs the initial movement of sediment particles. Given the semi-empirical nature of the Shields approach, it does not explicitly incorporate bed slopes. Therefore, to address this, a reduction factor (r) is used to compute the reduced critical shear stress (τ_c) [57–60]. This reduction factor (r) is multiplied by τ_0 to obtain the τ_c value, as presented in Eq. (8).

$$\tau_c = r\tau_0 \tag{8}$$

The present numerical model incorporates the analytical formulation of Dey [61] to determine the reduction factor (r), which is expressed as given in Eq. (9).

$$r = \frac{1}{(1-\eta\tan\phi)\tan\phi}\left\{-\left(\sin\theta + \eta\tan^2\phi\sqrt{\cos^2\theta - \sin^2\alpha}\right) + \left[\left(\sin\theta + \eta\tan^2\phi\sqrt{\cos^2\theta - \sin^2\alpha}\right)^2 + (1-\eta\tan^2\phi)(\cos^2\theta\tan^2\phi - \sin^2\alpha\tan^2\phi - \sin^2\theta - \sin^2\alpha)\right]^{0.5}\right\} \tag{9}$$

Here, η is the drag force upon inertia forces, θ is the longitudinal angle, α is the transverse angle, and ϕ is the angle of repose.

The sand-slide algorithm reduces bed shear stress by preventing excess sediment slip when the bed slope exceeds ϕ [62]. In such cases, the slope is adjusted by −2 deg, as suggested by Roulund et al. [63]. The computed effective stresses and critical bed stresses are coupled with the bedload calculation approach. This incorporates the application of the van Rijn formulas [64] to ensure the accurate computation of bedload, given in Eq. (10).

$$\frac{q_{b,i}}{d_i^{1.5}\sqrt{\frac{(\rho_s-\rho)g}{\rho}}} = 0.053\frac{\left(\frac{\tau-\tau_{c,i}}{\tau_{c,i}}\right)^{2.1}}{\left[\left(\frac{\rho_s/(\rho_w-1)g}{\nu^2}\right)^{1/3}\right]^{0.3}} \tag{10}$$

where $\tau_{c,i}$ is the critical bed shear stress, ρ_s is the sediment density, and d_i is the median sediment particle diameter.

Furthermore, the suspended sediment load transport is calculated using the standard convection–diffusion formulation [65], provided in Eq. (11).

$$\frac{\partial c}{\partial t} + u_j\frac{\partial c}{\partial x_j} + w_s\frac{\partial c}{\partial z} = \frac{\partial}{\partial x_j}\left(\Gamma\frac{\partial c}{\partial x_j}\right) \tag{11}$$

where c represents the sediment concentration and w_s is the sediment particle fall velocity. The value of the diffusion constant (Γ) is thought to be equal to the value of eddy viscosity [66].

The bottom suspended load concentration (c_b) and the zero vertical sediment flow at the free surface serve as the equation's boundary condition. According to van Rijn [65], sediment concentration along the bed (c_b) may be calculated as given in Eq. (12).

$$c_b = 0.015\frac{d_{50}}{a}\left(\frac{T^{1.5}}{D_*^{0.3}}\right) \tag{12}$$

in which a is the suspended sediment load datum level, and D_* is the sediment particle parameter, given in Eq. (13).

$$D_* = d_{50}\left[\frac{(s-1)g}{\nu^2}\right]^{1/3} \tag{13}$$

The Exner formulation is utilized to compute the bed elevation changes. This method is based on the concept of sediment mass conservation [38]. The Exner's equation used for the calculation of bed elevation changes is given in Eq. (14).

$$(1-n)\frac{\partial z_b}{\partial t} = -\frac{\partial q_{b,x}}{\partial x} - \frac{\partial q_{b,y}}{\partial z} - E + D \tag{14}$$

where q_b represents the bedload transport rate, while n denotes the porosity of sediment particles. Additionally, z_b signifies the local bed surface elevation, and E represents the erosion rate, with D indicating the deposition rate from suspended sediments.

2.3 Numerical Model Setup and Boundary Conditions. To model combined wave–current flows, a numerical wave tank (NWT) can be employed as a cost and time-efficient tool, replacing the physical modeling [45]. The traditional numerical wave tank used for simulating experimental conditions requires resource allocation, incurs considerable costs, and demands a substantial time investment. Therefore, a truncated-size numerical wave tank [46,67] is utilized in this study.

In the present study, the scour around a square pile in wave–current flows is investigated using an NWT of 3.5 m × 1 m × 0.7 m, as shown in Fig. 1. The inflow boundary condition is set as a uniform flow, while atmospheric pressure is assumed at the free surface. In NWT simulations, second-order Stokes waves along with the Dirichlet boundary condition are generated at one end of a confined domain (inlet) and subsequently absorbed at the opposite end (outlet). It is essential to avoid wave reflection from the absorption end to ensure accurate wave hydrodynamics and sediment transport in the numerical domain. The present NWT generates waves using the relaxation method [68] and encounters wave reflection at the end of the NWT using the active wave absorption method. The top boundary, located in the

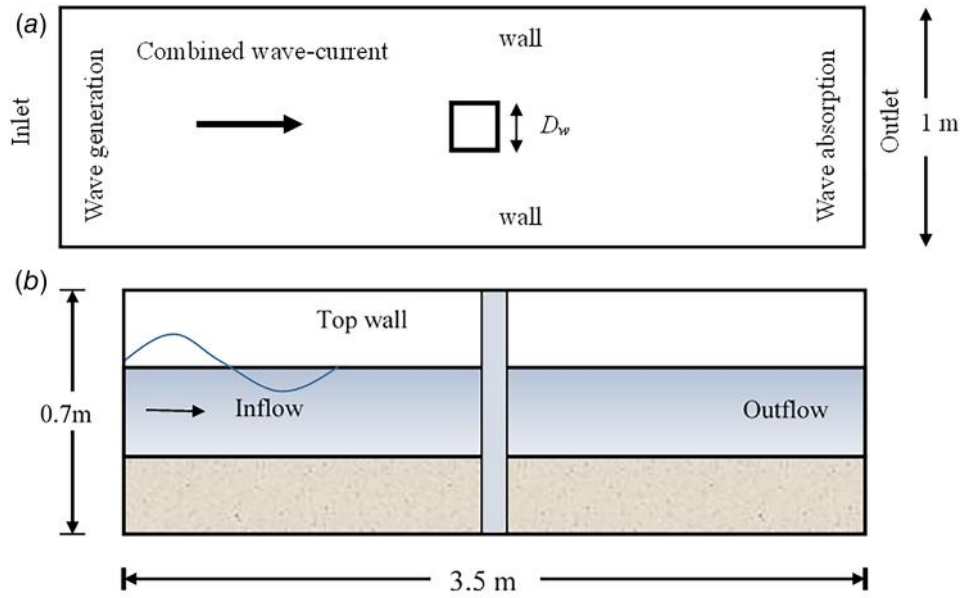

Fig. 1 Numerical wave tank with boundary conditions

Table 1 Details of the experiments used for model validation

Cases	D_w (m)	d_{50} (mm)	H (m)	T_w (s)	U_w (m/s)	U_c (m/s)	U_{cw}	KC	Exp. S (cm)	Sim. S (cm)	Error %
Current (Fig. 2) [70]	0.08	0.75	–	–	–	0.28	1	–	12.5	12.6	0.8
Current (Fig. 3) [18]	0.16	0.85	–	–	–	0.22	1	–	8	7.72	3.5
Wave (Fig. 4) [28]	0.01	0.18	0.12	4.5	0.32	–	0	14.6	2.5	2.45	2
Wave (Fig. 5) [29]	0.02	0.18	0.18	1.4	0.31	–	0	22	0.35	0.4	14.3
Wave–current (Fig. 6) [71]	0.05	0.40	0.07	1	0.08	0.21	0.71	1.67	6.6	6.75	2.3
Wave–current (Fig. 7) [21]	0.08	0.38	0.033	1.4	0.30	0.23	0.43	1.28	3.36	3.28	2.4

Note: H represents the wave height, and S/D_w represents the normalized pile scour depth.

air phase, is designated as a symmetry plane, where vertical velocities and horizontal velocity gradients are set to zero. The ghost cell immersed boundary approach [69] is used to simulate solid boundaries within the NWT. Additionally, the side walls are treated as rough walls, imposing a no-slip boundary condition that defines velocities near the wall.

2.4 Numerical Model Validation and Grid Convergence Study. The present study employs a novel sediment transport module within REEF3D, an open-source CFD code based on wave–current environments. However, the numerical model must be validated in order to demonstrate accuracy in predicting equilibrium scour depth in wave-only, steady flow, and combined wave–current flow. In steady current, the numerical results were validated with the experimental data on the temporal change in pile scour, as Xiao et al. [70] observed for circular piles and Khosronejad et al. [18] for square piles. Experimental data from Sumer et al. [28] for circular piles and Sumer et al. [29] for square piles were used to validate numerical results for the wave-only condition. Furthermore, the numerical model was validated against experimental data from Ref. [71] for circular pile scour in the combined wave −current condition. Due to the unavailability of the square pile scour experimental dataset in the combined wave–current condition, we performed additional validation with grid convergence for circular pile scour against experimental data of Qi and Gao [21]. The details of the experiments utilized in this study for the model validation are provided in Table 1.

2.4.1 Steady Current. In steady current, the numerical results of temporal scour variations around the monopile were validated with experimental results of Xiao et al. [70], as shown in Fig. 2. The numerical results show a scour depth of 12.6 cm, which coincides with the experimental finding of 12.5 cm, corresponding to a minimal percentage error of just 0.8%. This close correspondence demonstrates the accuracy of the numerical model in capturing the scour process. Furthermore, the temporal evolution of monopile scour predicted by the simulations shows good consistency with

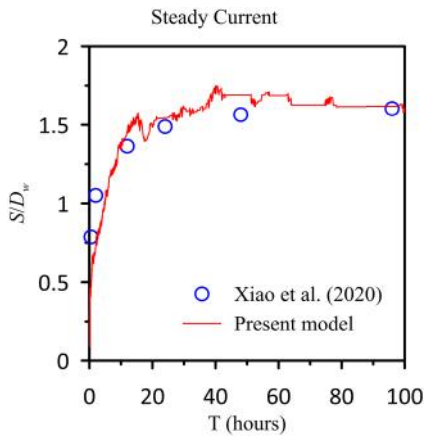

Fig. 2 Numerical results validated with Xiao et al.'s [70] experimental data of temporal scour variations at the monopile in a steady current

the experimental observations reported by Xiao et al. [70], indicating that the model reliably reproduces both the magnitude and development of scour over time.

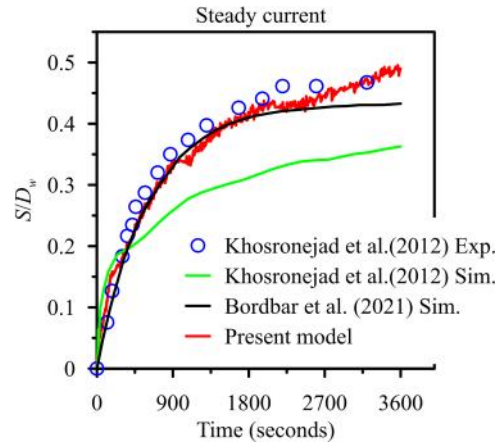

Fig. 3 Numerical results validated with Khosronejad et al.'s [18] experimental data of temporal scour variations at the square pile in a steady current

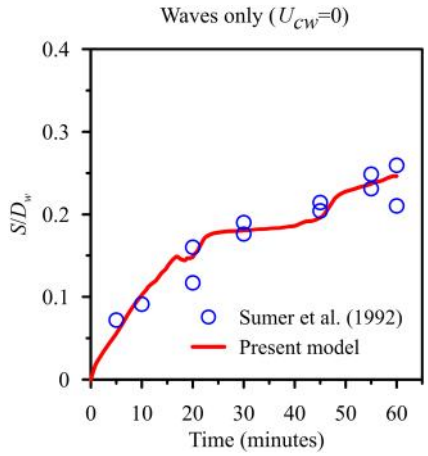

Fig. 4 Numerical results validated with Sumer et al.'s [28] experimental data of temporal scour variations at a circular pile in the wave condition

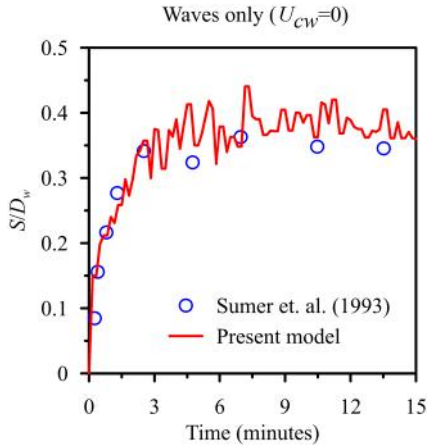

Fig. 5 Numerical results validated with Sumer et al.'s [29] experimental data of temporal change in square pile in the wave-only condition

Figure 3 illustrates the temporal scour variation around the square pile in a steady current during a physical modeling duration of $T = 1$ h. The numerical simulation predicted an equilibrium scour depth of 8 cm, which is in close agreement with the experimental value of 7.72 cm from Ref. [18], corresponding to a small percentage error of 3.5%. This close agreement highlights the accuracy of the numerical model under current only conditions. In addition, the present numerical results were compared with the findings from the studies of Khosronejad et al. [18] and Bordbar et al. [72]. The comparison demonstrates that the present model reproduces the observed scour patterns effectively and aligns well with the experimental data. Nevertheless, it is noted that the numerical predictions from both Refs. [72,18] tend to underestimate the temporal variations in scour development around the pile, whereas the present model captures these dynamics more accurately.

2.4.2 Wave-Only Condition. In the wave-only condition, the results of the present developed model were validated using the experimental results of Sumer et al. [28] for the temporal change in circular pile scour ($T = 1$ h), as shown in Fig. 4. The numerical simulation predicted an equilibrium scour depth of 2.45 cm, which is in close agreement with the experimentally measured value of 2.5 cm reported by Sumer et al. [28], corresponding to a

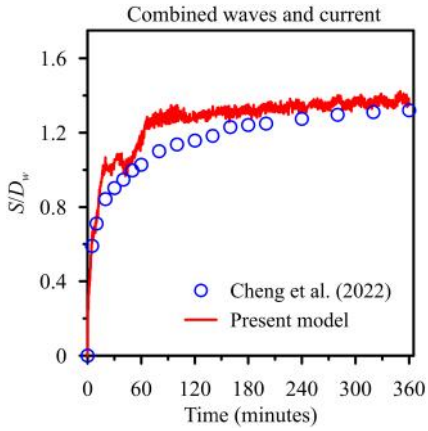

Fig. 6 Numerical results validated with Cheng et al.'s [71] experimental data of temporal scour variations in wave–current flows

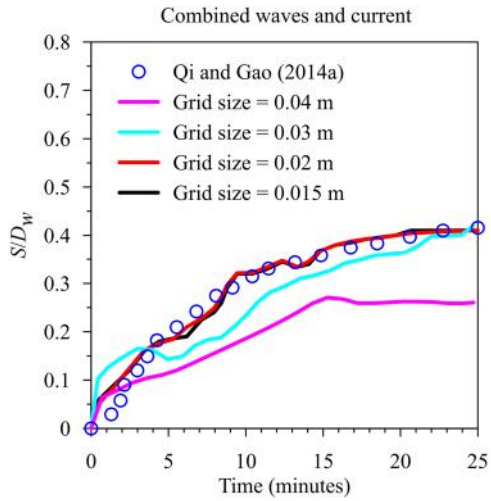

Fig. 7 Numerical results with grid convergence validation with Qi and Gao's [21] experimental results of temporal scour variations in wave–current flows

minimal percentage error of only 2%. This close correspondence demonstrates the reliability and accuracy of the developed model in capturing wave-induced scour processes. Moreover, the predicted temporal variation in scour depth closely follows the experimental trend, further confirming that the model effectively reproduces both the magnitude and the temporal development of scour around a circular pile under wave-only conditions.

Figure 5 illustrates the temporal scour variation at the square pile in the wave-only condition during a physical modeling duration of $T = 15$ min. The numerical model predicted an equilibrium scour depth of 4 mm, closely aligning with the experimental value of 3.5 mm, resulting in a higher percentage error of 14.3%. This larger relative error arises from the very small absolute scour depth, where minor deviations naturally produce higher percentage differences. Overall, the temporal evolution of scour predicted by the model aligns well with the experimental observations of Sumer et al. [29]. However, the numerical results show a slight variation in the temporal change of scour, which is mainly due to the erosive and deposition nature of oscillatory flow.

Table 2 Grid convergence metrics for equilibrium scour depth under different grid sizes

Grid size (m)	S/D_w	Percentage change versus previous grid
0.040	0.260	–
0.030	0.422	62.3
0.020	0.411	2.6
0.015	0.409	0.49

2.4.3 Combined Wave–Current Flows. In the combined wave–current environment, the present model observations were validated with the experimental findings of temporal change in circular pile scour ($T = 6$ h) observed by Cheng et al. [71], as shown in Fig. 6. The numerical simulation yielded an equilibrium scour depth of 6.75 cm, closely matching the experimental value of 6.6 cm, corresponding to a small percentage error of 2.3%. This close agreement demonstrates the model's capability to accurately capture the complex interactions between waves and currents. Furthermore, the temporal development of scour around the circular pile predicted by the model shows good consistency with the experimental observations during both the initial and equilibrium phases of scour. However, the numerical results throughout the scour-progressive phase show a modest overprediction, compared to experimental datasets.

The reliability of the numerical model in the combined wave–current environment was enhanced by validating its scour predictions against the experimental results of Qi and Gao [21]. The present numerical model's predictions for pile scour were compared with experimental data from Qi and Gao [21] for combined wave–current flow, as illustrated in Fig. 7. Grid convergence analysis was performed to assess the impact of grid resolution on simulation accuracy and reliability. The study tested grid sizes of

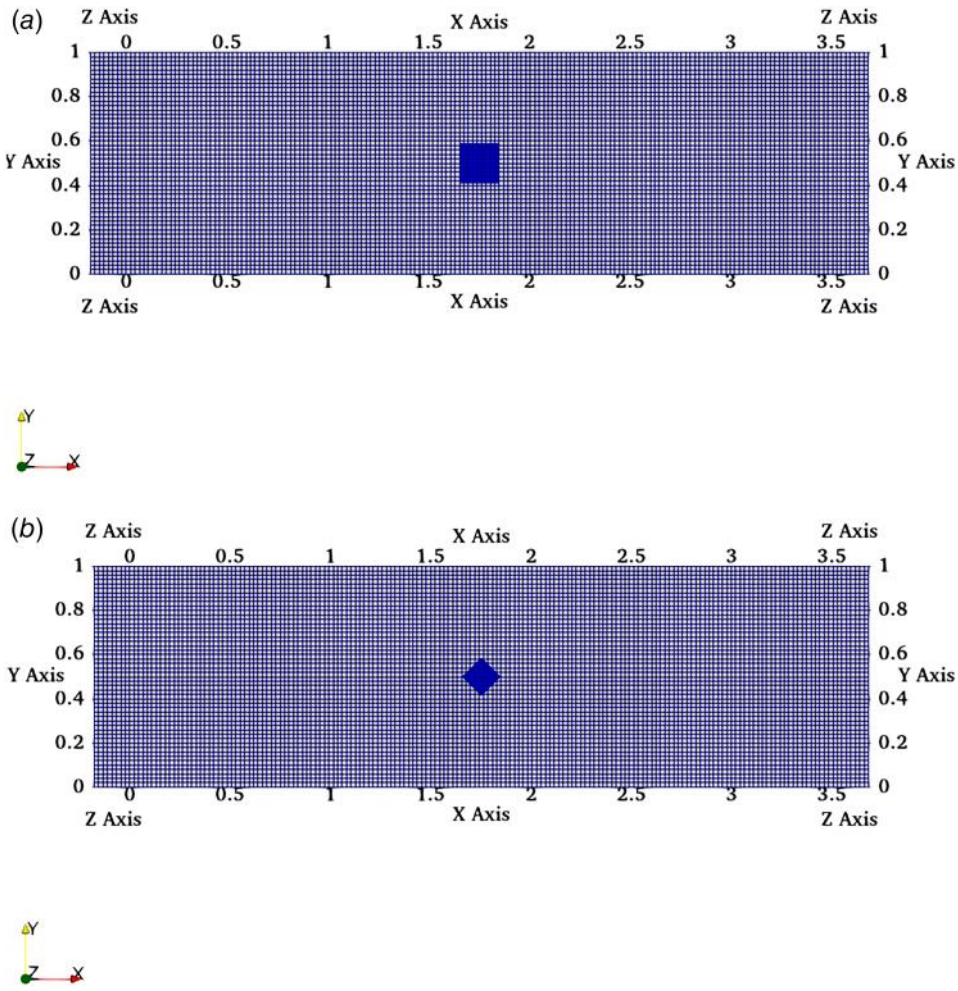

Fig. 8 Grid decompositions of numerical wave tank with square piles of (*a*) 90 deg and (*b*) 45 deg orientations

4, 3, 2, and 1.5 cm, revealing that coarser grids of 4 cm and 3 cm underestimated temporal scour depths. Further refining the grid to 2 cm yields an equilibrium scour depth of 3.28 cm, which closely matches the experimental value of 3.36 cm, corresponding to a percentage error of 2.4%, thereby confirming the model's capability under combined wave–current conditions. Using a 1.5 cm grid does not significantly improve accuracy compared to the 2 cm grid but greatly increases computation time and cost. Therefore, a grid size of 2 cm was selected for analyzing the pile scour process in the wave–current condition.

Table 3 Hydraulic and wave parameters used in the numerical simulations

Case #	D_w (m)	H (m)	U_w (m/s)	U_c (m/s)	U_{cw}	Fr_a	KC	45 deg (S/D_w)	90 deg (S/D_w)	% change in S/D_w
1	0.18	0.051	0.156	–	–	0.07	3.9	0.076	0.046	+65.2
2	0.18	0.051	0.156	0.039	0.2	0.10	3.9	0.099	0.072	+37.5
3	0.18	0.051	0.156	0.104	0.4	0.15	3.9	0.125	0.118	+5.9
4	0.18	0.051	0.156	0.234	0.6	0.25	3.9	0.200	0.228	−12.3
5	0.14	0.058	0.179	–	–	0.10	5.75	0.100	0.067	+49.3
6	0.14	0.058	0.179	0.045	0.2	0.14	5.75	0.141	0.110	+28.2
7	0.14	0.058	0.179	0.119	0.4	0.20	5.75	0.195	0.176	+10.8
8	0.14	0.058	0.179	0.268	0.6	0.33	5.75	0.294	0.309	−4.9
9	0.08	0.058	0.178	–	–	0.13	10	0.128	0.105	+21.9
10	0.08	0.058	0.178	0.045	0.2	0.18	10	0.179	0.166	+7.8
11	0.08	0.058	0.178	0.119	0.4	0.26	10	0.213	0.245	−13.1
12	0.08	0.058	0.178	0.267	0.6	0.43	10	0.383	0.400	−4.3
13	0.08	0.10	0.320	–	–	0.23	18	0.339	0.400	−15.3
14	0.08	0.10	0.320	0.080	0.2	0.32	18	0.405	0.435	−6.9
15	0.08	0.10	0.320	0.213	0.4	0.47	18	0.416	0.478	−13
16	0.08	0.10	0.320	0.480	0.6	0.77	18	0.441	0.480	−8.1

Note: Every case was conducted for both square piles with 45 deg and 90 deg orientations.

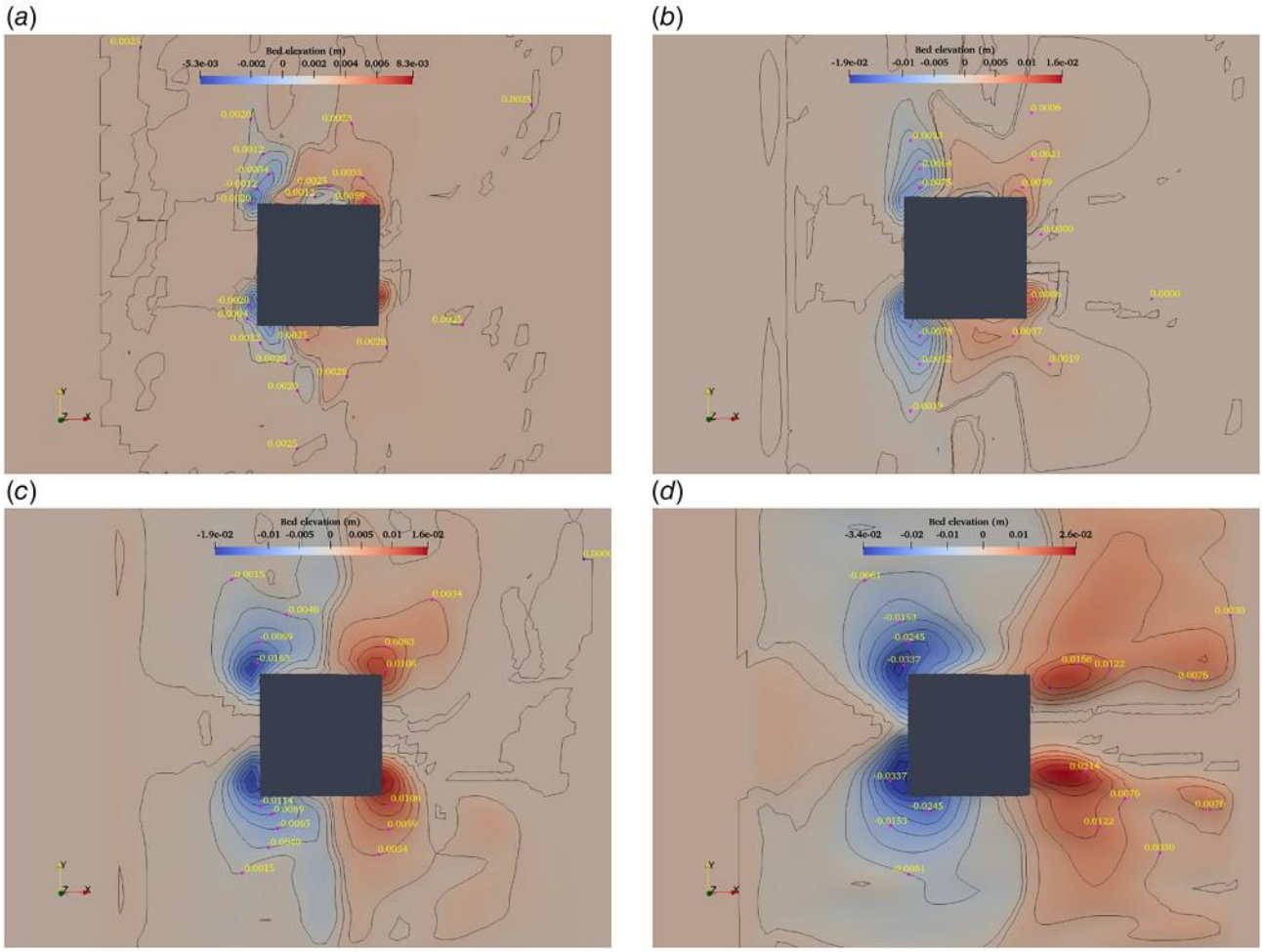

Fig. 9 The contour plots of bed topography around 90 deg and 45 deg oriented square piles under varying U_{cw} parameters for KC = 3.9

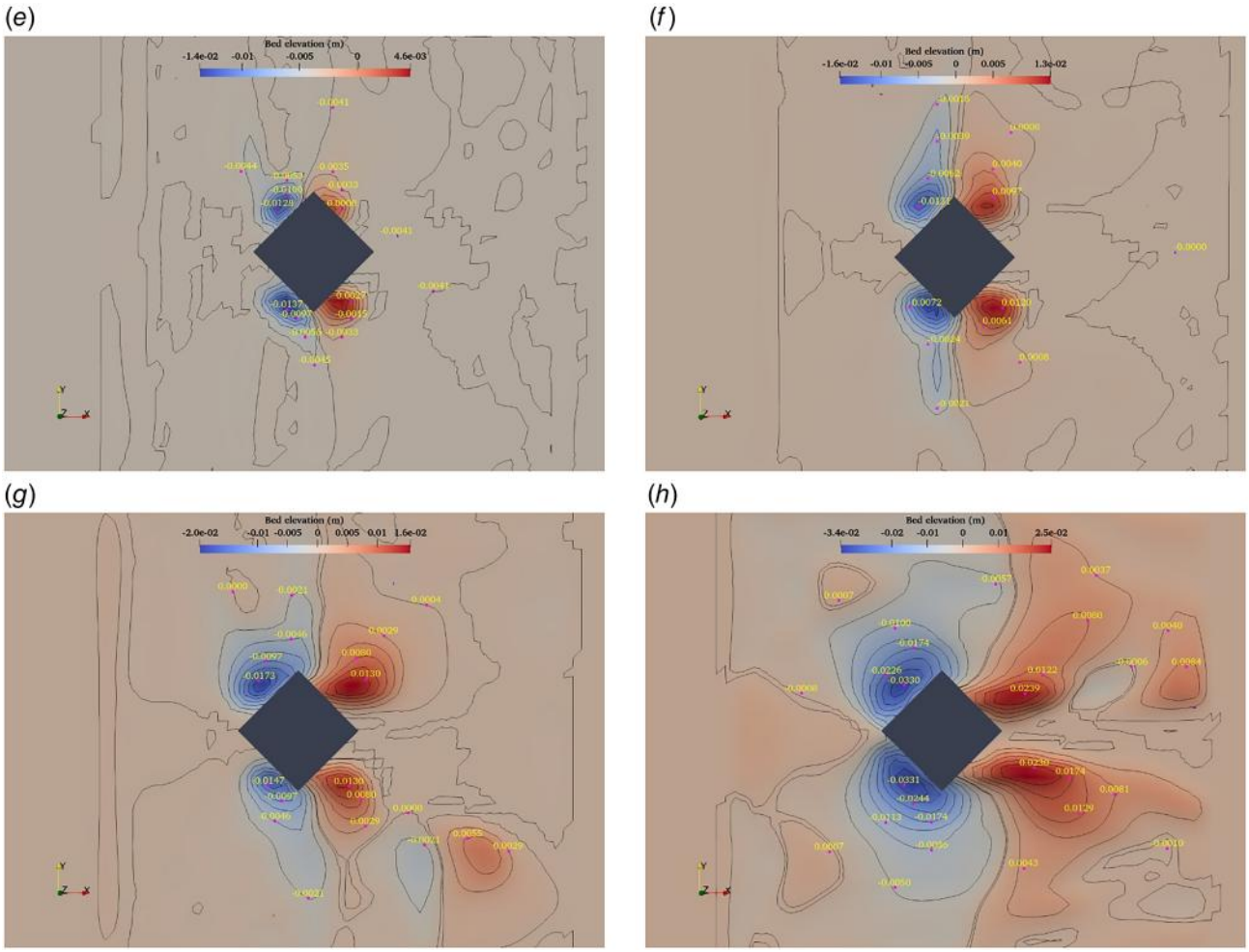

Fig. 9 ***Continued***

A quantitative grid convergence analysis was also performed to assess the influence of spatial resolution on the predicted equilibrium scour depth (S/D_w). The results, as summarized in Table 2, show that as the grid is refined from 0.04 m to 0.03 m, the equilibrium scour depth increases significantly (by approximately 62.3%), indicating that the coarsest grid is unable to adequately resolve the near-bed flow structures and sediment transport processes. Further refinement from 0.03 m to 0.02 m results in only a 2.6% change in S/D_w, while an additional refinement to 0.015 m leads to a negligible change of 0.49%. These results clearly demonstrate that the solution becomes nearly grid-independent for grid sizes finer than 0.02 m. Considering both accuracy and computational efficiency, the grid size of 0.02 m was selected for all subsequent simulations, ensuring a reliable representation of the scour process around the pile.

A uniform staggered Cartesian [10,42,46,73] grid size of 2 cm with a stretching ratio of 1 is utilized to perform all the numerical simulations in this study. In REEF3D, it can be observed that the uniform finer grid of 2 cm accurately captures the flow features, such as separation zones, wake formation, and vortical flow structures in the numerical wave tank. The uniform grid also provides better simulation results of complex sediment transport and scour phenomena. The grid resolution at solid boundaries is crucial for capturing near-wall turbulent structures accurately. In the present study, the grid resolution near solid boundaries is maintained at 2 cm in wall units. The grid decomposition of NWT, which consists of a square pile with orientations of (a) 90 deg and (b) 45 deg, is shown in Fig. 8.

3 Results and Discussion

Square piles can be used with different orientations based on the stability needs of the structure. The present study deals with the complex scour phenomenon around the square piles of 45 deg and 90 deg orientations in combined wave–current flows, which has not been extensively explored in the existing literature.

To explore square pile scour with different orientations in wave–current environments, all simulations are performed with an NWT of 3.5 m × 1 m × 0.7 m. The numerical experiments were conducted using a median sediment size (d_{50}) of 0.18 mm with a sand bed thickness of 15 cm and a critical Shields parameter (θ_{cr}) of 0.047. The flow water depth (h) was maintained at 25 cm for all the numerical simulations. To obtain a fixed KC number, the pile width (D_w) for both orientations of square piles is kept the same. The numerical simulations were conducted with three different pile widths: 0.18 m, 0.14 m, and 0.08 m. In the present study, the pile Reynolds number is varied between 14,240 and 28,080 for both orientations of the square pile. The value of the wave parameter (kh) was set at 0.2247 in every numerical simulation. Throughout the numerical experiments, the wavelength (L) of the second-order Stokes waves remains constant at 6.98 m. The wave period is also kept constant, equal to 4.5 s. The U_{cw} parameter was systematically varied between 0 and 0.6. The wave height (H) was varied between 0.506 and 0.10 m to achieve different KC numbers (i.e., 3.9, 5.75, 10, and 18), each corresponding to a distinct vortex flow regime as described by Sumer et al. [31]. These flow regimes are as follows: (a) for $2.8 < KC < 4$, a pair of symmetric vortices formed due to flow separation behind the

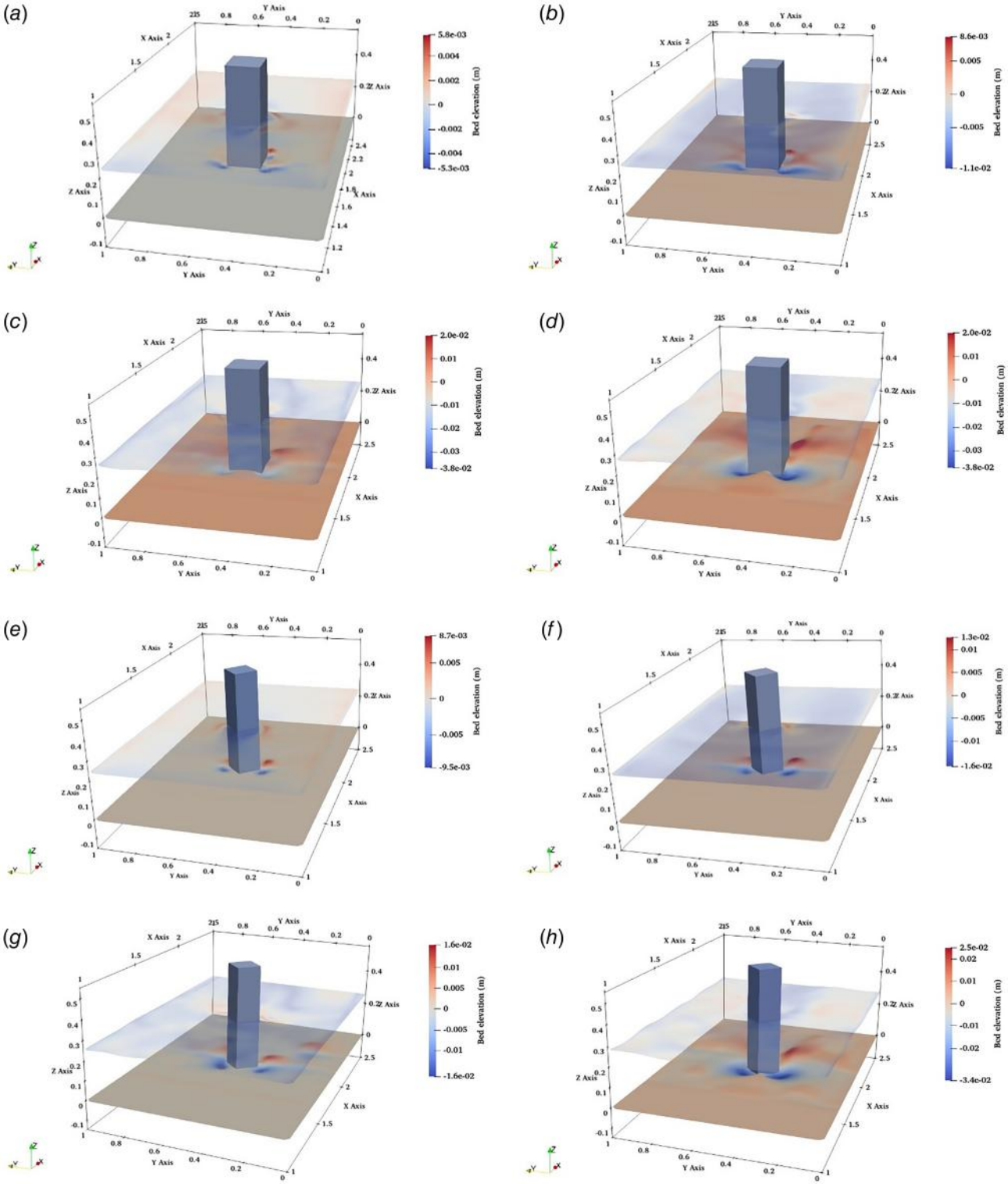

Fig. 10 Three-dimensional view of the sediment bed and free surface at the square pile with 90 deg and 45 deg orientation under different U_{cw} parameters for a fixed KC = 3.9

piles; (b) in the range of $4 < KC < 6$, the symmetry of these vortex pairs is disrupted, though they remain attached, indicating that vortex shedding has not yet begun; (c) for $6 < KC < 17$, vortex shedding occurs, with one vortex being shed during each half cycle; (d) for $17 < KC < 23$, vortex shedding persists, with two vortices being shed in each half cycle, resulting in an extended lee-wake behind the pile, as also reported by Williamson [74].

To investigate the S/D_w values around 45 deg and 90 deg oriented square pile in wave–current flows, a total of 32 numerical experiments were performed. All the numerical experiments reached equilibrium scour depth in 3600 s, represented as T_e. The numerical parameters used to examine S/D_w around a square pile with 45 deg and 90 deg orientations in a wave–current environment are summarized in Table 3.

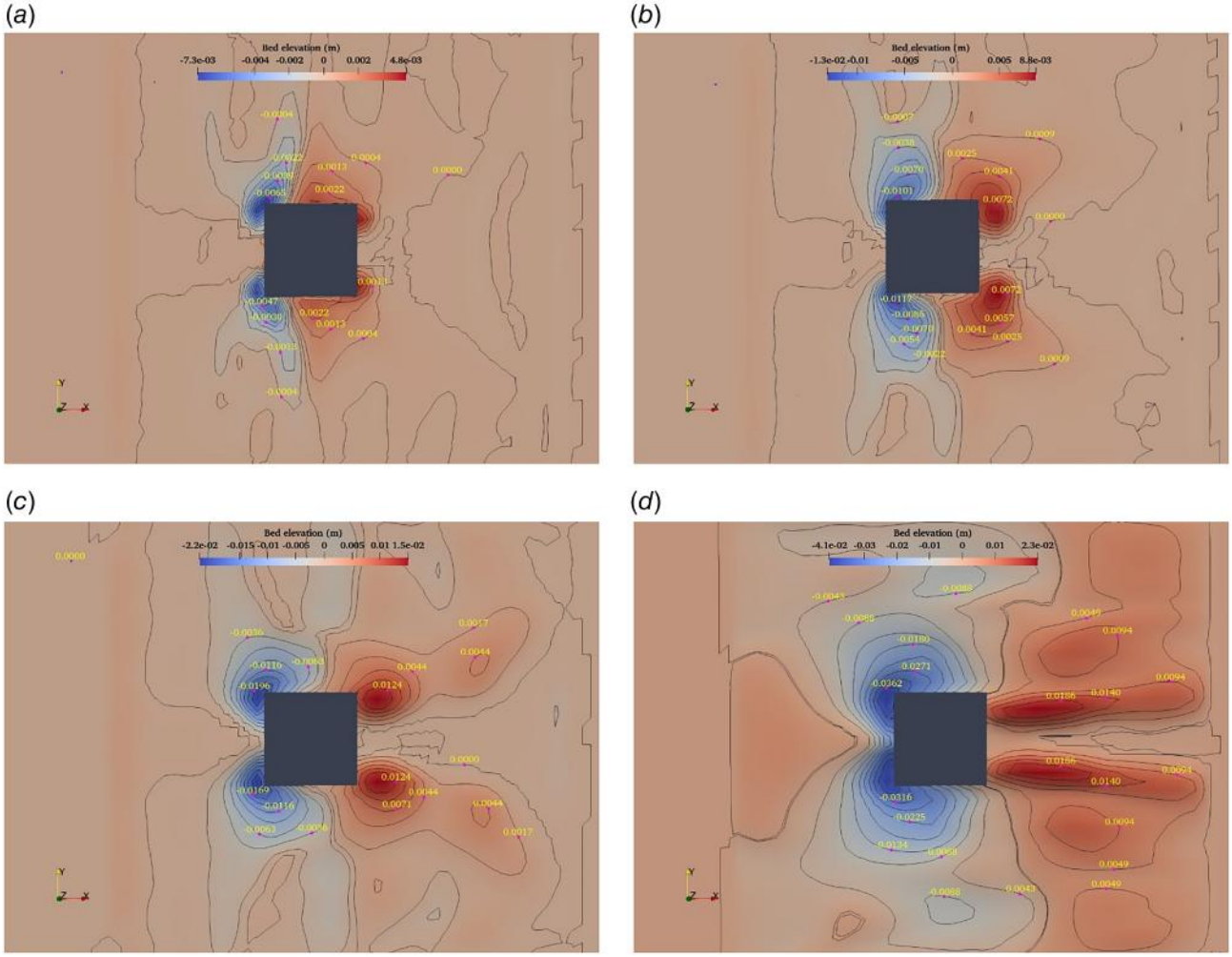

Fig. 11 The contour plots of bed topography around 90 deg and 45 deg oriented square piles under varying U_{cw} parameters for KC = 5.75

3.1 Bed Topography at Different Keulegan–Carpenter Regimes. This section examines the bed topography around square piles with 45 deg and 90 deg orientations under varying U_{cw} parameters and different KC regimes. The focus is on understanding how combined wave–current flows affect the scour patterns around these piles in different KC regimes. The analysis highlights the impact of pile orientation and flow dynamics on scour patterns, providing insights into the complex interplay of hydrodynamic forces and sediment response.

The contour plots of bed topography around the square piles with 90 deg and 45 deg orientations under varying U_{cw} parameters for KC = 3.9 are shown in Fig. 9. The contours with negative values, indicating scour, while the contour with positive values, indicating deposition of sediment particles around the pile. For the wave-only condition ($U_{cw} = 0$), both pile orientations exhibit minor frontal scour holes upstream. The pile with 90 deg orientation shows greater scour depth at its upstream corners than at its stagnation point, indicating a stronger flow acceleration effect at the corners. However, the square pile with 45 deg orientation exhibits more symmetrical scour and deposition patterns, with reduced scour depth compared to the pile of 90 deg orientation. As the U_{cw} parameter increases, the scour depth also increases, and downstream sand dunes emerge. For $U_{cw} = 0.6$, strong currents generate large frontal scour holes and twin horn-shaped dunes downstream in both orientations of the square pile. However, the scour for 45 deg oriented square pile remains more symmetric compared to the 90 deg orientation, aligning with observations by Zhao et al. [75].

Figure 10 presents a realistic three-dimensional view of the sediment bed and free surface with velocity magnitude of square pile with 90 deg and 45 deg orientation using the LSM at KC = 3.9. The results show nearly identical maximum scour and deposition magnitudes, which can be attributed to the high velocities along the sides of the piles. This results in the entrainment of sediments from the upstream side and their transportation into the downstream region characterized by lower velocities. Soulsby and Whitehouse [32] observed the emergence of ripples on the bed surface when the Shields parameter fell within the range of $\theta_{cr} \leq \theta \leq 0.8$. However, in the present study with square pile (45 deg and 90 deg), no ripple formation was observed despite the Shields parameter falling within the same range (Figs. 10(*a*)–10(*h*)). This discrepancy could be attributed to the influence of the pile geometry on the flow patterns and sediment transport. The shape and orientation of the piles can affect how water and sediment interact with the bed.

Figure 11 represents the contour plots of bed topography around 90 deg and 45 deg oriented square piles under varying U_{cw} parameters for KC = 5.75. A symmetrical scour pattern is evident at the upstream side edges of both square piles with 90 deg (Figs. 11(*a*)–11(*d*)) and 45 deg orientations (Figs. 11(*e*)–11(*h*)). In the wave-only condition, a minor upstream scour hole is observed, accompanied by the deposition of sediments just beneath the square pile oriented at 90 deg (Fig. 11(*a*)) and 45 deg (Fig. 11(*e*)). Similarly to KC number = 3.9, the increase in U_{cw} parameter leads to a larger scour depth, extended scour

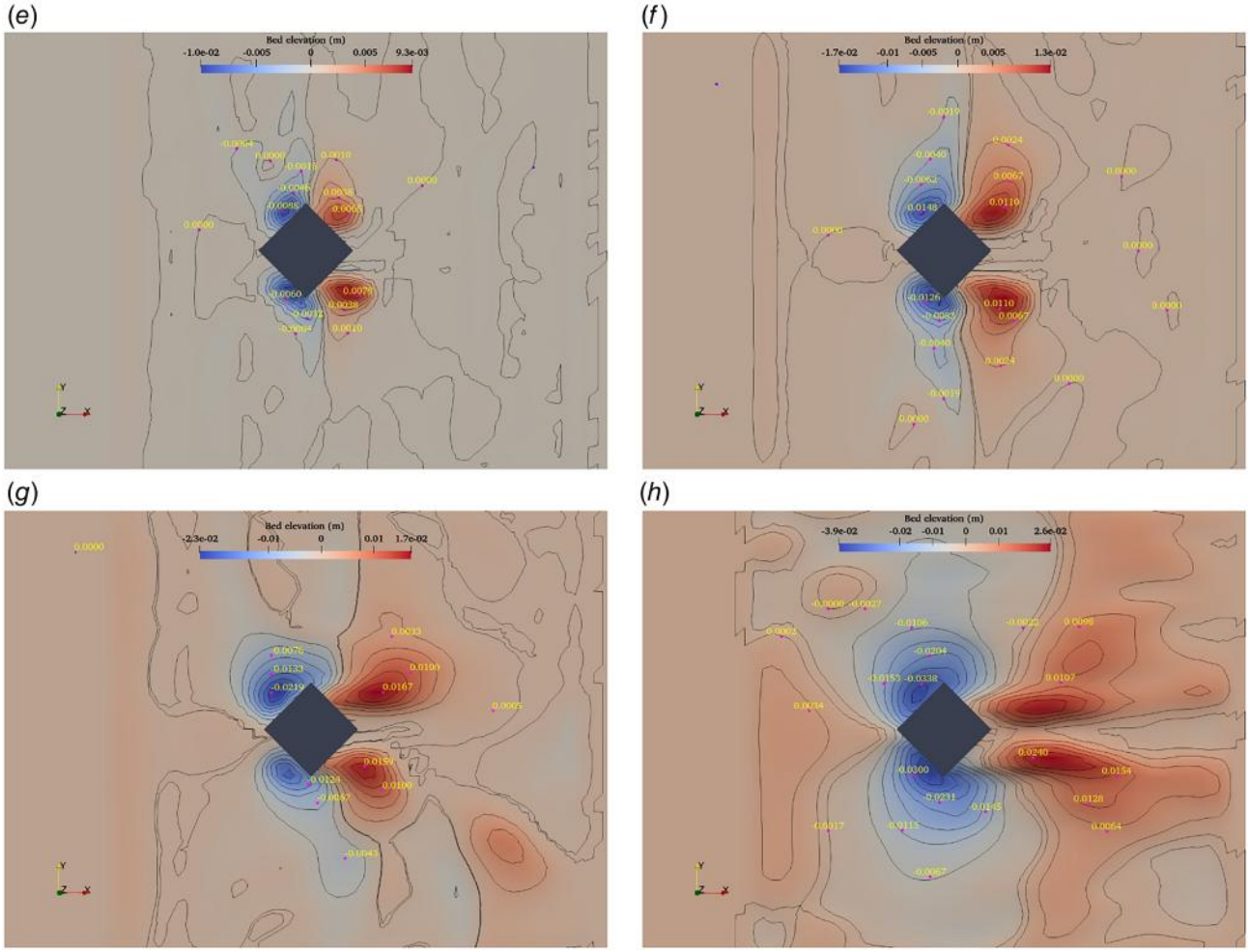

Fig. 11 ***Continued***

hole width, and more deposition in the downstream region of both orientations. Finally, in the case of $U_{cw} = 0.6$, the maximum scour depth and more prominent and extended twin horn-shaped dunes were observed downstream, particularly near the square pile of 90 deg orientation. However, the square pile with a 45 deg orientation preserves more symmetrical scour patterns but has a comparative scour depth formation than the square pile with a 90 deg configuration. Sumer et al. (1993) observed the absence of vortex shedding phenomenon in square piles with 90 deg orientation until KC < 11 and for square piles with 45 deg orientation until KC < 4. They noted that the vortices formed behind the piles draw sediment grains into their core region yet fail to transport them away due to the lack of shedding. At KC = 5.75, the initiation of vortex shedding for square piles with 45 deg orientation results in deeper and wider scour profiles compared to KC = 3.9, driven by higher bed shear stress, increased sediment entrainment, and more dynamic flow–structure interactions.

Figure 12 presents a realistic three-dimensional view of the sediment bed and free surface of the square pile with 90 deg and 45 deg orientation using the LSM at KC = 5.75. The results show nearly identical maximum scour and deposition magnitudes, which can be attributed to the high velocities along the sides of the piles. At KC = 5.75, the Shields parameter does not fall within the specified range of $\theta_{cr} \le \theta \le 0.8$ in wave-only conditions; hence, no ripple formation was observed (Figs. 12(*a*) and 12(*e*)). Furthermore, in the wave–current flow, the Shields parameter falls in the range of $\theta_{cr} \le \theta \le 0.8$, leading to the observation of small ripples. Notably, an increase in current velocity corresponds to an increase in the magnitude of ripples (Figs. 12(*d*) and 12(*h*)).

The contour plots of bed topography around 90 deg and 45 deg oriented square pile under varying U_{cw} parameters for KC = 10 are shown in Fig. 13. In the case of KC = 10, the effects of vortex shedding become more apparent on bed topography. Similar to KC numbers 3.9 and 5.75, a small scour depth formation is in front of the pile and slight deposition downstream of both the square pile orientations in $U_{cw} = 0$. With an increase in U_{cw} parameter, a wider and larger scour depth was obtained upstream of both square pile orientations, while larger dunes were observed downstream, which are larger than the case of KC numbers 3.9 and 5.75. In the case of $U_{cw} = 0.4$ and 0.6, elongated twin horn-shaped dunes were evident, with the 90 deg orientation of the square pile exhibiting slightly deeper and more extensive scour compared to the 45 deg orientation. The alternate development of wing scour holes and deposition is noticeable in a square pile oriented at 45 deg, primarily attributed to the vortex shedding phenomenon, as noted by Sumer et al. (1993). However, in the case of a square pile oriented at 90 deg, vortex shedding initiates after the KC number exceeds 11.

Figure 14 depicts the three-dimensional view of the sediment bed and free surface of a square pile with 90 deg and 45 deg realistically using the LSM for KC = 10. The results show nearly identical maximum scour and deposition magnitudes, which can be attributed to the high velocities along the sides of the piles. At KC = 10, the Shields parameter does not fall within the specified range of $\theta_{cr} \le \theta \le 0.8$ in wave-only conditions; hence, no ripple formation was observed (Figs. 14(*a*) and 14(*e*)). Furthermore, in the wave–current flow, the Shields parameter falls in the range of $\theta_{cr} \le \theta \le 0.8$, leading to the observation of ripples.

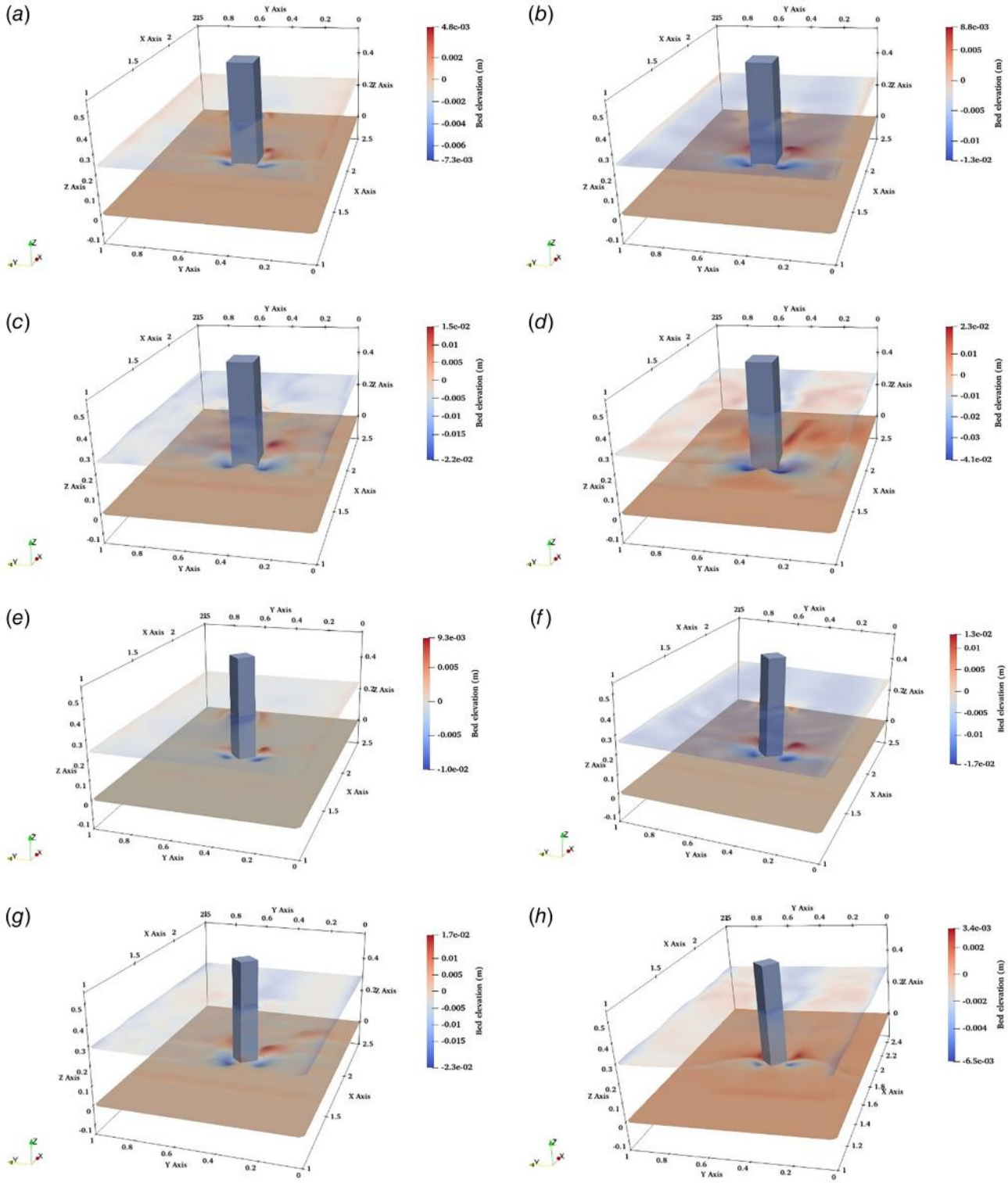

Fig. 12 Three-dimensional view of the sediment bed and free surface at the square pile with 90 deg and 45 deg orientation under different U_{cw} parameters for a fixed KC = 5.75

Notably, an increase in current velocity corresponds to an increase in the magnitude of ripples (Figs. 14(*d*) and 14(*h*)). Furthermore, it can be observed that more pronounced, deeper, and wider scour formation occurs when waves are superimposed on currents. This phenomenon is primarily attributed to the influence of strong currents, which generate a stronger HSV around both orientations of square pile.

Similarly, the contour plots of bed topography around 90 deg and 45 deg oriented square pile under varying U_{cw} parameters for KC number = 18 are shown in Fig. 15. Similar to other KC numbers (3.9, 5.75, and 10), a symmetric scour pattern was found at the upstream edges of the square pile oriented at 90 deg and 45 deg in the wave-only condition. However, the square pile with a 90 deg orientation forms wider and larger upstream scour

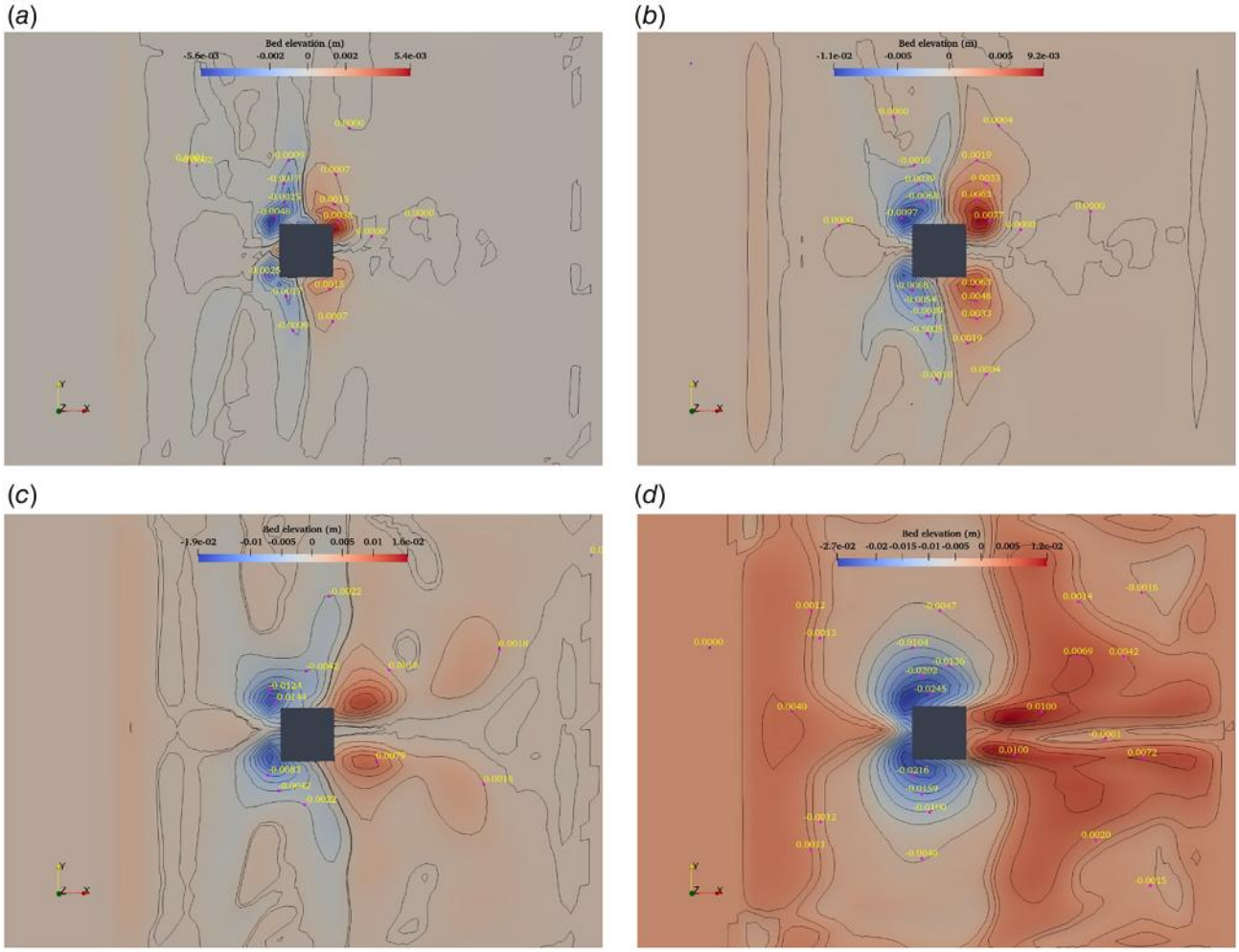

Fig. 13 The contour plots of bed topography around 90 deg and 45 deg oriented square piles under different U_{cw} parameters for KC = 10

holes and downstream sand dunes than the 45 deg orientation. According to Gautam et al. [39], waves with a high KC number (KC = 18) interact with weak, mild, or strong currents, leading to the development of strong wave-generated currents. As a result, larger lee-wake vortices and HSV are generated, causing greater scour depth formation around the square piles oriented at 90 deg and 45 deg. However, the effect of the U_{cw} parameter becomes negligible at KC = 18, with respect to the lower KC numbers studied in the present study.

Figure 16 depicts the three-dimensional view of the sediment bed and free surface of the square pile with 90 deg and 45 deg orientation for KC = 18 using the LSM. The results show nearly identical maximum scour and deposition magnitudes, which can be attributed to the high velocities along the sides of the piles. For KC = 18, the Shields parameter for both wave-only and combined wave–current conditions falls within the specified range of $\theta_{cr} \leq \theta \leq 0.8$. Despite this, no ripples were observed on the bed topography for both 90 deg (Figs. 16(*a*)–16(*d*)) and 45 deg orientation (Figs. 16(*e*)–16(*h*)). This absence may be attributed to the fact that, at higher KC numbers, the flow regime undergoes a transition where other forces and phenomena, such as turbulence, wave breaking, or shear forces, exert greater influence. These factors can significantly impact the formation and stability of ripples. Moreover, the elevated KC numbers indicative of increased flow momentum may disrupt ripple formation as the flow energy becomes directed toward alternative forms of water surface disturbance.

3.2 Temporal Change in S/D_w Parameter at Different Keulegan–Carpenter Regimes. The temporal change in S/D_w parameter at different KC regimes provides insight into the evolution of scour under varying flow conditions. The rate and extent of scour formation are strongly influenced by the KC number and U_{cw} parameter, which govern the flow oscillation and sediment transport. Therefore, this section highlights the critical role of KC numbers and U_{cw} parameter on the temporal evolution of scour depth around different orientations of the square pile (90 deg and 45 deg).

Figure 17 depicts the temporal change in S/D_w parameter of square pile oriented at 90 deg (shown in Fig. 17(*a*)) and 45 deg (shown in Fig. 17(*b*)) for varying U_{cw} parameters at KC = 3.9. The temporal change in square pile scour is shown by for varying U_{cw} parameters of 0, 0.2, 0.4, and 0.6, respectively. For $U_{cw} = 0$, the minimum S/D_w values of 0.0462 and 0.076 were observed for square piles oriented at 90 deg and 45 deg, respectively. The generation of smaller wake vortices under wave-only conditions causes reduced pile scour compared to wave–current conditions, as suggested by Gautam et al. [39]. In combination of waves with weak current ($U_{cw} = 0.2$), the S/D_w values of 0.072 and 0.099 were obtained for square piles oriented at 90 deg and 45 deg, respectively. Similarly, the combination of waves with a weak current leads to a gentle increase in the scour depth for both orientations of square with respect to $U_{cw} = 0$.

Furthermore, for $U_{cw} = 0.4$, the S/D_w values of 0.118 and 0.125 were obtained for square piles oriented at 90 deg and 45 deg,

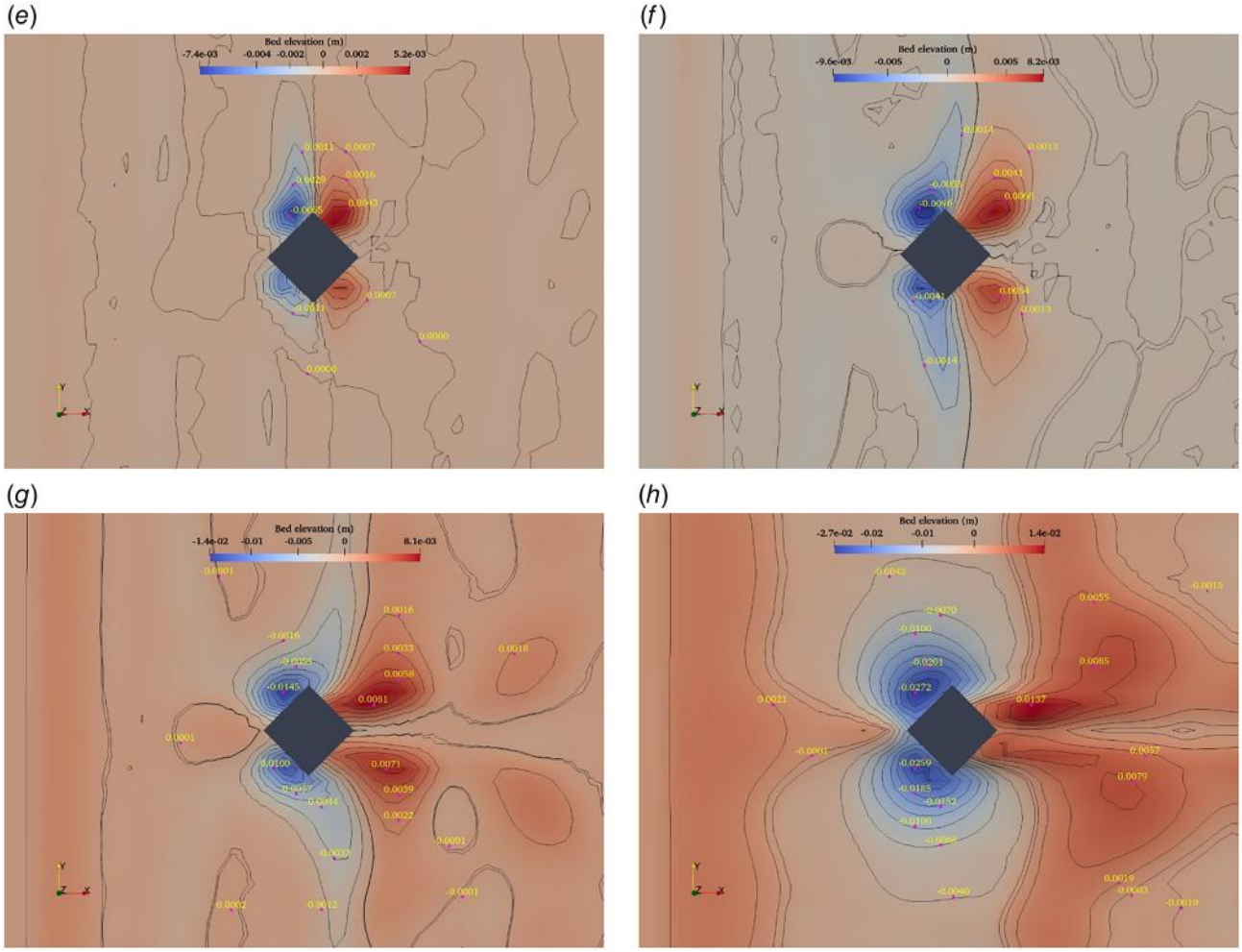

Fig. 13 ***Continued***

respectively. In this case, the presence of a mild current component increases the impact of U_{cw}, leading to an increase in scour depth compared to the scenario of $U_{cw} = 0.2$. Finally, for $U_{cw} = 0.6$, the S/D_w values of 0.228 and 0.200 were observed for square piles oriented at 90 deg and 45 deg, respectively. In this case, the strong current component increases the intensified effects of waves and currents acting together, leading to a significant increase in scour compared to $U_{cw} = 0.2$ and 0.4. It can be observed that the square pile oriented at 45 deg has a higher S/D_w value in comparison to the square pile oriented at 90 deg under different U_{cw} parameters varying from 0 to 0.4. However, the square pile oriented at 45 deg has a lower S/D_w than the square pile oriented at 90 deg under waves superimposed on a strong current ($U_{cw} =$ 0.6) at KC = 3.9. A possible reason for this difference is the dominance of strong currents that led to strong HSV generation, which raised the pile scour depth fast and substantially.

Figure 18 depicts the temporal change S/D_w value of square pile oriented at 90 deg (shown in Fig. 18(*a*)) and 45 deg (shown in Fig. 18(*b*)) for varying U_{cw} parameters at KC = 5.75. In the wave-only condition, the minimum S/D_w values of 0.067 and 0.100 were observed for square piles oriented at 90 deg and 45 deg, respectively. The development of smaller wake vortices under wave-only conditions leads to reduced scour compared to wave–current conditions. For $U_{cw} = 0.2$, the S/D_w values of 0.110 and 0.141 were obtained for square piles oriented at 90 deg and 45 deg, respectively. The combination of waves with weak currents leads to a gentle increase in the scour depth with respect to the wave-only condition ($U_{cw} = 0$). Similarly, for $U_{cw} = 0.4$, the S/D_w values of 0.176 and 0.195 were obtained for square piles oriented at 90 deg and 45 deg, respectively. In this case, the presence of a mild current component increases the impact of U_{cw} parameter, resulting in an increase in scour compared to the scenario of waves coupled with weak currents ($U_{cw} = 0.2$).

Furthermore, for $U_{cw} = 0.6$, the S/D_w values of 0.309 and 0.294 were obtained for square piles oriented at 90 deg and 45 deg, respectively. In this case, the presence of a strong current component increases the intensified effects of waves and currents acting together, leading to a significant increase in scour formation compared to the scenario of waves coupled with weak or mild currents. It can be observed that the square pile with orientation of 45 deg has a higher S/D_w value in comparison to the square pile with orientation of 90 deg under U_{cw} with values of 0–0.4. However, the square pile with an orientation of 45 deg has a lower S/D_w value than the square pile under waves combined with strong current ($U_{cw} = 0.6$) for KC = 5.75. It can be observed that the effect of U_{cw} parameter (0.2 and 0.4) on the S/D_w value is much less in comparison to the case of $U_{cw} = 0.6$.

Figure 19 depicts the temporal change in S/D_w values at square pile oriented at 90 deg (shown in Fig. 19(*a*)) and 45 deg (shown in Fig. 19(*b*)) under varying U_{cw} parameters for KC number = 10. In the wave-only condition, the minimum S/D_w values of 0.105 and 0.128 were observed for square piles oriented with 90 deg and 45 deg, respectively. This happens due to the generation of smaller wake vortices around the pile under the wave-only condition, which may result in comparatively lower scour formation around the pile in comparison to the combined wave–current condition. For $U_{cw} = 0.2$, the S/D_w values of 0.166 and 0.179 were obtained for square piles oriented with 90 deg and 45 deg,

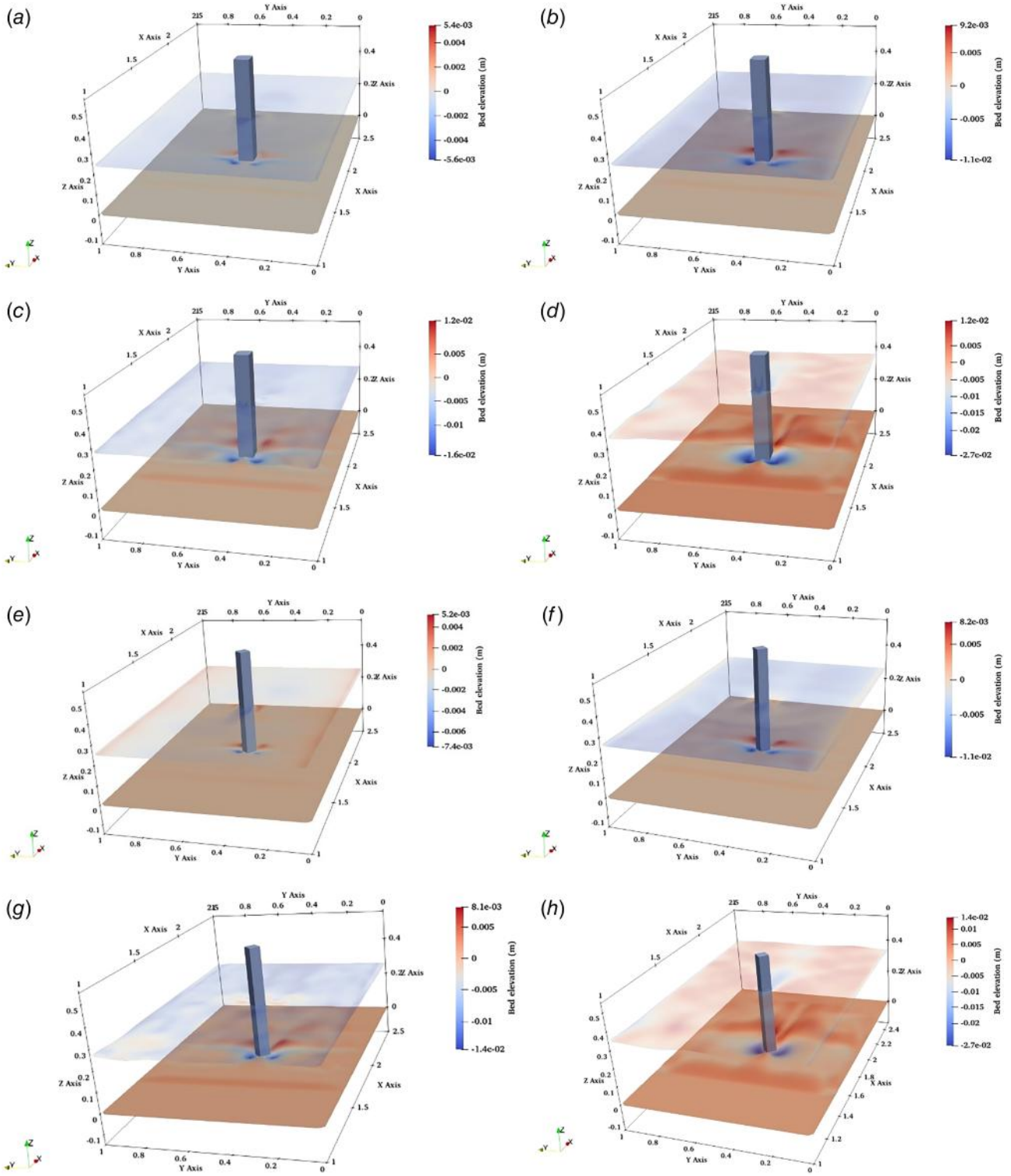

Fig. 14 Three-dimensional view of the sediment bed and free surface at the square pile with 90 deg and 45 deg orientation under different U_{cw} parameters for a fixed KC = 10

respectively. The results indicate that the increase in U_{cw} parameter leads to higher scour depth. Furthermore, in the case of $U_{cw} = 0.4$, S/D_w values of 0.245 and 0.213 were observed for square piles oriented with 90 deg and 45 deg, respectively. In this case, the presence of a mild current component increases the impact of U_{cw} parameter, resulting in an increase in scour compared to the scenario of waves coupled with weak currents ($U_{cw} = 0.2$).

Finally, for $U_{cw} = 0.6$, the S/D_w values of 0.400 and 0.383 were observed for square piles oriented with 90 deg and 45 deg, respectively. In this case, the presence of a strong current component increases the intensified effects of waves and current acting together, leading to a significant increase in scour compared to the scenario of waves combined with weak or mild currents. It can be observed that the square pile oriented at 45 deg has a

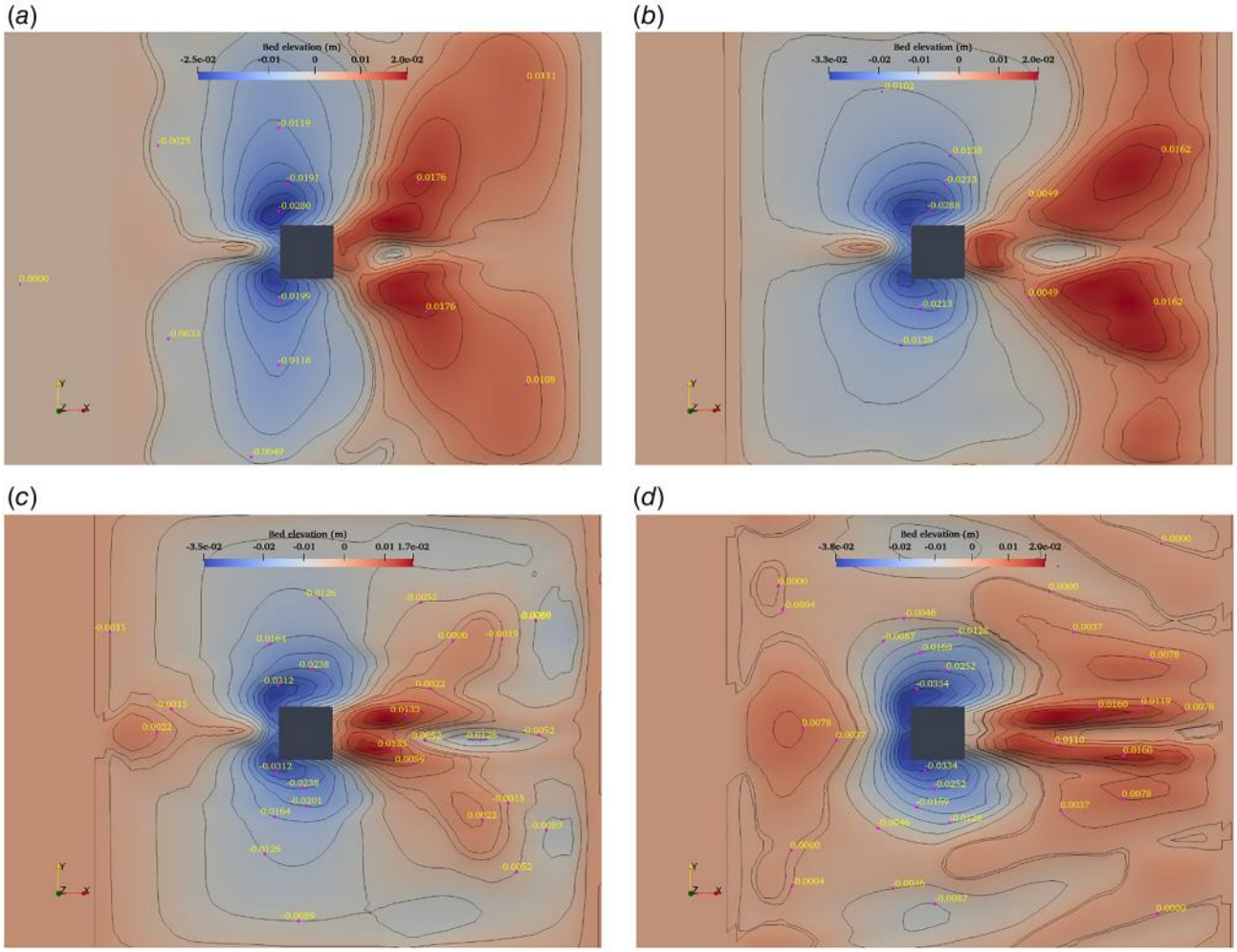

Fig. 15 The contour plots of bed topography around 90 deg and 45 deg oriented square piles under varying U_{cw} parameters for KC = 18

higher S/D_w value in comparison to the square pile oriented at 90 deg under U_{cw} values 0 and 0.2. However, the square pile oriented at 45 deg has a lower S/D_w value than the square pile oriented at 90 deg under waves superimposed on a mild and strong current ($U_{cw} = 0.4$ and 0.6) for a fixed KC number 10. It is evident that waves combined with mild or weak currents have a significantly less impact on the scour depth than waves combined with strong currents.

Figure 20 depicts the temporal change in S/D_w at square pile oriented with 90 deg (shown in Fig. 20(*a*)) and 45 deg (shown in Fig. 20(*b*)) under varying U_{cw} parameters for KC = 18. In the wave-only condition, the minimum S/D_w values of 0.400 and 0.339 were observed for square piles oriented at 90 deg and 45 deg, respectively. The generation of smaller wake vortices around the pile under the wave-only condition results in lower scour hole formation in comparison to the wave–current condition. For $U_{cw} = 0.2$, the S/D_w values of 0.435 and 0.405 were observed for square piles oriented at 90 deg and 45 deg, respectively. The increase in U_{cw} parameter from 0 to 0.2 leads to a gentle increase in the scour depth with respect to $U_{cw} = 0$. Similarly, for $U_{cw} = 0.4$, the S/D_w values of 0.478 and 0.416 were obtained for square piles oriented at 90 deg and 45 deg, respectively. In this case, the presence of a mild current component increases the impact of U_{cw} parameter, resulting in a gentle increase in scour compared to the scenario of waves coupled with weak currents ($U_{cw} = 0.2$).

Furthermore, for $U_{cw} = 0.6$, the S/D_w values of 0.480 and 0.441 were obtained for square piles oriented at 90 deg and 45 deg, respectively. In this case, the presence of a strong current component increases the effects of wave–current flows and leads to a higher increase in scour depth compared to the $U_{cw} = 0$, 0.2, and 0.6 till $t/T_e = 0.7$ (2520 s) in both orientations of the square pile. However, as the t/T_e exceeds 0.7, there is a fall in equilibrium scour depth, which may occur due to the backfilling of sediments. It can be observed that the square pile with orientation of 90 deg has a higher S/D_w value in comparison to the square pile oriented at 45 deg for all U_{cw} values at KC = 18. The effect of U_{cw} becomes almost negligible compared to other KC numbers used in the present study. This observation suggests that for higher KC numbers, such as KC = 18, the current component's role becomes insignificant compared to smaller KC numbers, such as KC = 3.9, 5.75, and 10. The findings obtained in this study are consistent with the findings obtained by Sumer and Fredsøe [23].

3.3 Effect of U_{cw} and KC Number on Square Pile Scour.

Sumer and Fredsøe [23] reported that the nondimensional parameters such as U_{cw} and KC number affect the formation of scour in wave–current flows. The present study investigates the pile scour phenomenon with varying U_{cw} (0, 0.2, 0.4, and 0.6) and KC numbers (3.9, 5.75, 10, and 18). Therefore, the influence of U_{cw} and KC numbers on S/D_w values for both orientations of square piles (90 deg and 45 deg orientations) is shown in Fig. 21.

The variation of S/D_w value with U_{cw} parameter for square piles oriented at 90 deg is shown in Fig. 21(*a*). A gentle increase in S/D_w values can be found for low KC regimes with an increase in U_{cw} value from 0 to 0.4. As U_{cw} parameters increase from 0.4 to 0.6,

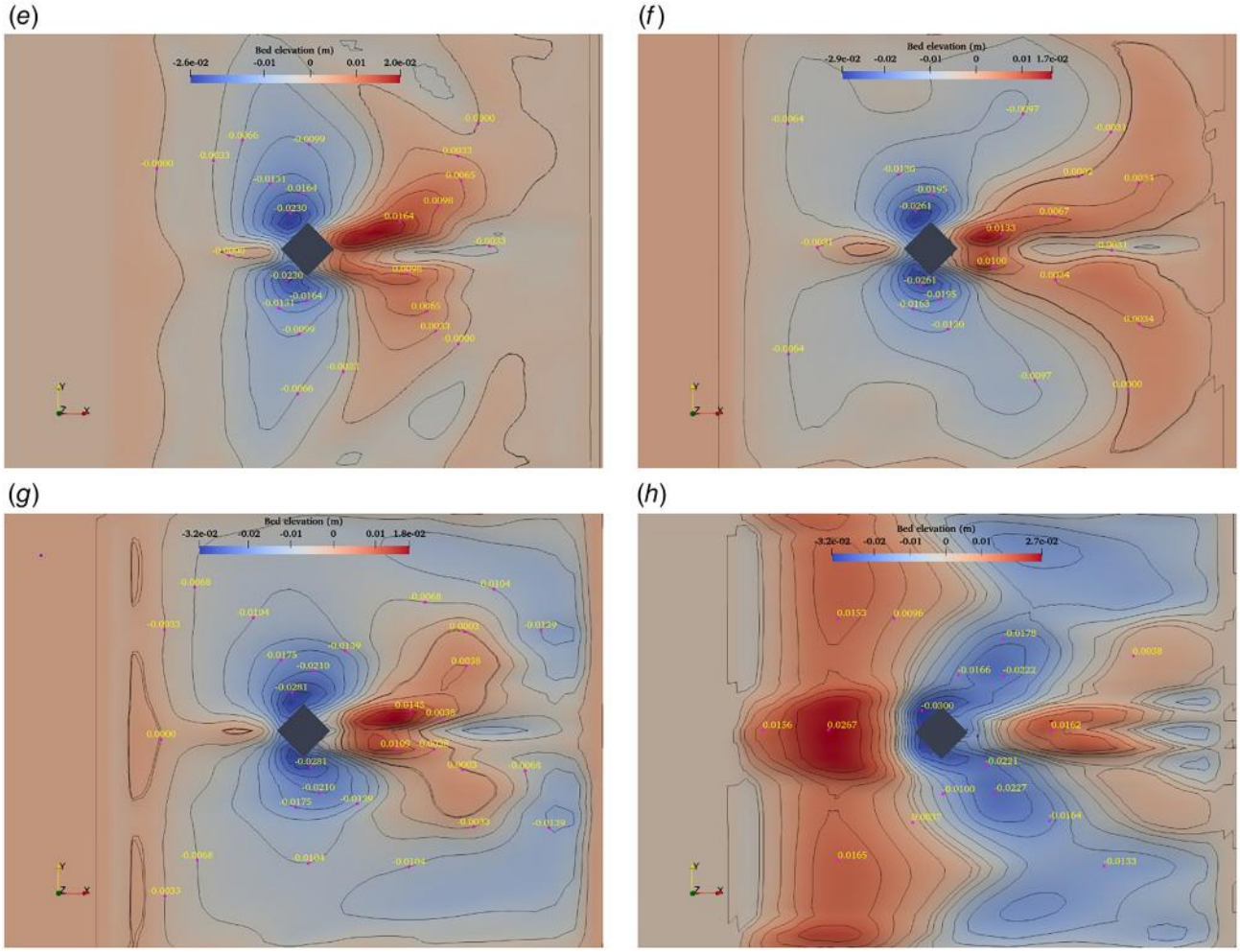

Fig. 15 ***Continued***

the S/D_w values also increase rapidly for low KC numbers (e.g., KC = 3.9, 5.75, and 10). This is mainly due to the presence of strong HSV in front of the pile, even in the case of a weak current. However, a mild increase in S/D_w values can be observed for a higher KC regime (e.g., KC = 18) with an increase in U_{cw} value from 0 to 0.2 at the square pile oriented at 90 deg. Furthermore, the S/D_w value becomes almost constant with an increase in U_{cw} values from 0.2 to 0.6 in the higher KC regime. It is evident that the S/D_w value increases with an increase in KC number for the 90 deg oriented square pile for a fixed U_{cw}. Similarly, the effect of the U_{cw} parameter on S/D_w can be observed for the square pile oriented at 45 deg (Fig. 21(*b*)). However, a larger scour depth can be observed around the square pile oriented at 45 deg compared to the square pile oriented at 90 deg in the lower KC regime (KC < 10).

The variation of S/D_w with KC number for a square pile oriented at 90 deg is shown in Fig. 21(*c*). It is evident that for a specific value of U_{cw}, an increase in the KC number results in an increase in the S/D_w values. The measured S/D_w values versus the KC number exhibit distinct curves for different values of U_{cw}. As KC increases to 100 (steady current case), these curves converge toward a common asymptotic value. This indicates that regardless of the specific range of U_{cw}, the ultimate scour depth reaches a constant level at higher KC values. According to Sumer et al. [31], the higher U_{cw} with a smaller KC number can generate a stronger HSV, leading to a deeper scour formation around the pile. Similarly, the KC number equals 3.9 with a strong current superimposed on waves ($U_{cw} = 0.6$) and has a higher S/D_w value of 0.2277 than the KC number of 10 with waves combined with weak currents ($U_{cw} = 0.2$).

Similarly, the effect of the KC number on S/D_w can be observed for the square pile oriented at 45 deg (Fig. 21(*d*)). However, a larger scour depth can be observed around the square pile oriented at 45 deg compared to the square pile oriented at 90 deg in the lower KC regime (KC < 10). The results obtained in the present investigation validate the effect of U_{cw} and KC numbers on S/D_w values and are in line with previous studies by Sumer et al. [29]. In conclusion, the study investigates the effect of KC number and combined wave–current (U_{cw}) parameter on square pile scour, which demonstrates that the increase in KC and U_{cw} parameter increases the scour around piles with different bed topographies.

3.4 Effect of Fr_a on Pile Scour. To determine the S/D_w values in wave–current flows, the Fr_a is identified as an essential parameter by Qi and Gao [22]. The generation of HSV and wake vortex is mostly responsible for scour hole formation around piles, which are strongly related to the Fr_a. The variation of S/D_w with respect to the Fr_a value is shown in Fig. 22.

The variation of S/D_w with respect to Fr_a for both orientations of square pile in the combined wave–current condition is shown in Fig. 22. It is evident that the S/D_w value rises rapidly initially for Fr_a (i.e., 0–0.4) for both square pile orientations. Further increase in the Fr_a value leads to an asymptotic or constant value of the S/D_w parameter. For the square pile oriented at 90 deg, the S/D_w

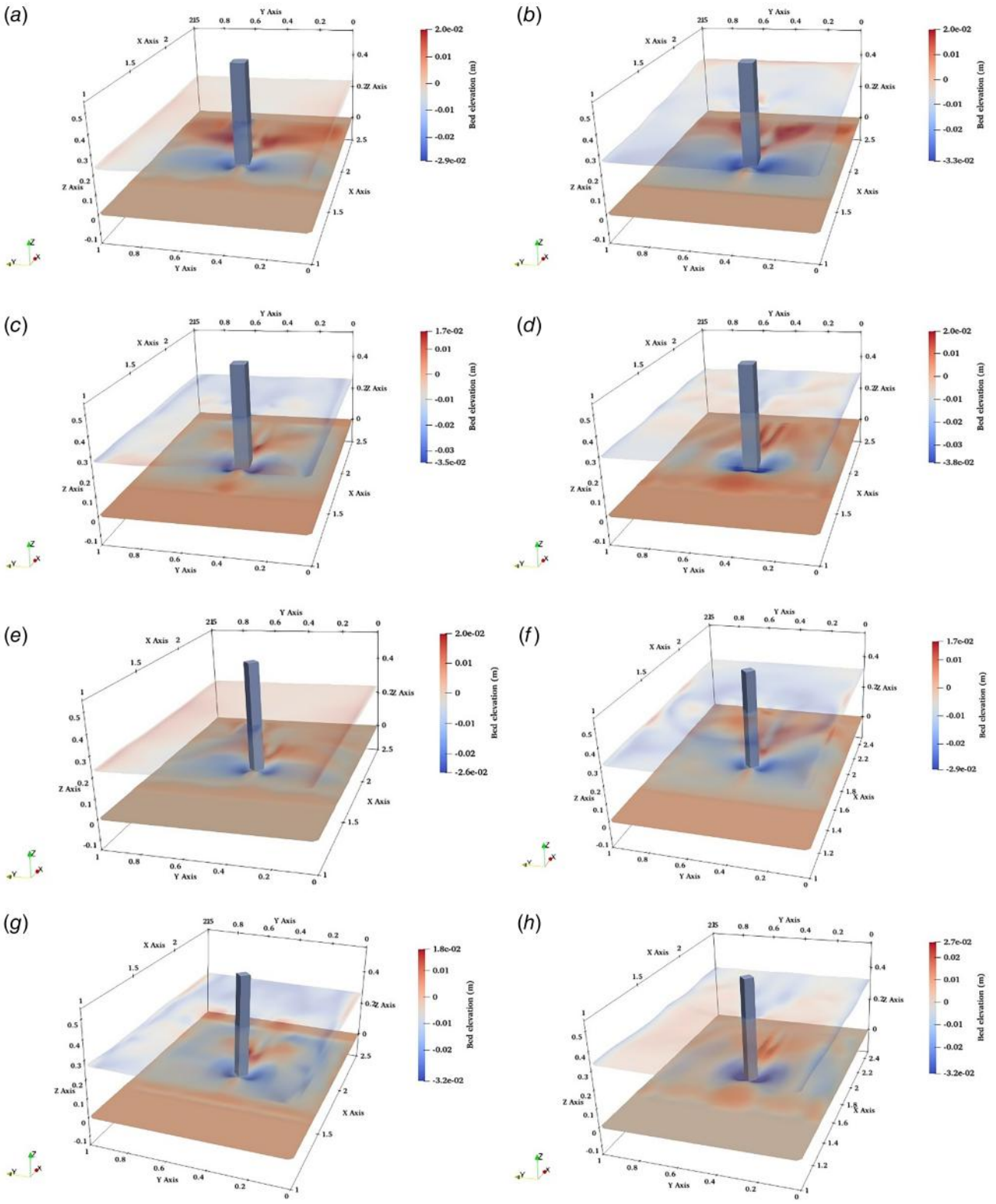

Fig. 16 Three-dimensional view of the sediment bed and free surface at the square piles with 90 deg and 45 deg orientation under different U_{cw} parameters for a fixed KC = 18

asymptotically approaches a value of 0.6, whereas for the square pile oriented at 45 deg, the asymptotic value is slightly lower, around 0.5. These differences highlight the influence of pile orientation on the S/D_w values. The numerical S/D_w values (shown in Fig. 22) can be expressed in terms of Fr_a for both orientations of square piles using the fitting curves provided in Eqs. (15) and (16), respectively.

$$S/D_w = 0.227 \times \ln(\mathrm{Fr}_a) + 0.592 \quad (0.075 < \mathrm{Fr_a} < 0.772,\ \ 3.9 < KC < 18) \tag{15}$$

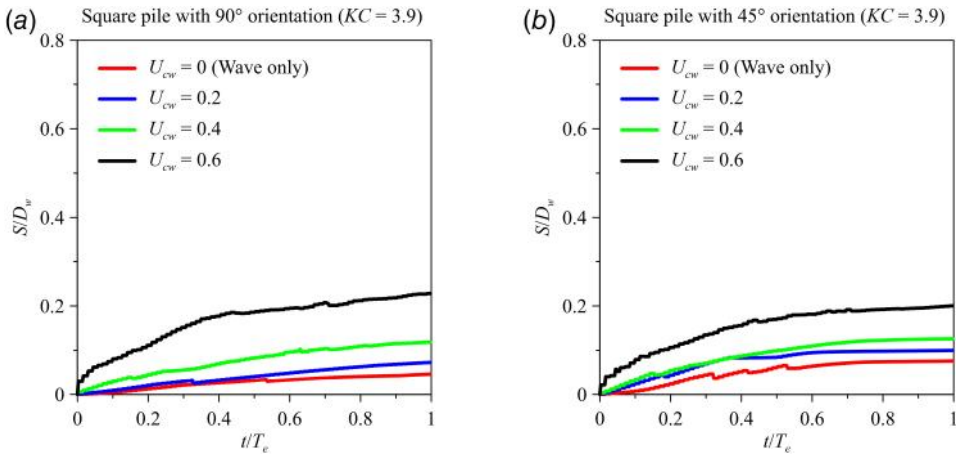

Fig. 17 Temporal change in S/D_w at square pile with (*a*) 90 deg and (*b*) 45 deg orientations for KC = 3.9

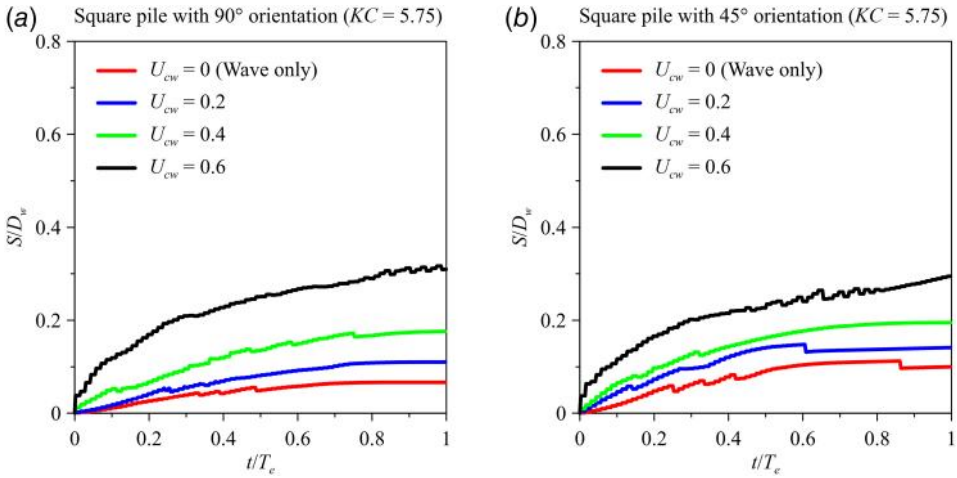

Fig. 18 Temporal change in S/D_w at square pile with (*a*) 90 deg and (*b*) 45 deg orientations for KC = 5.75

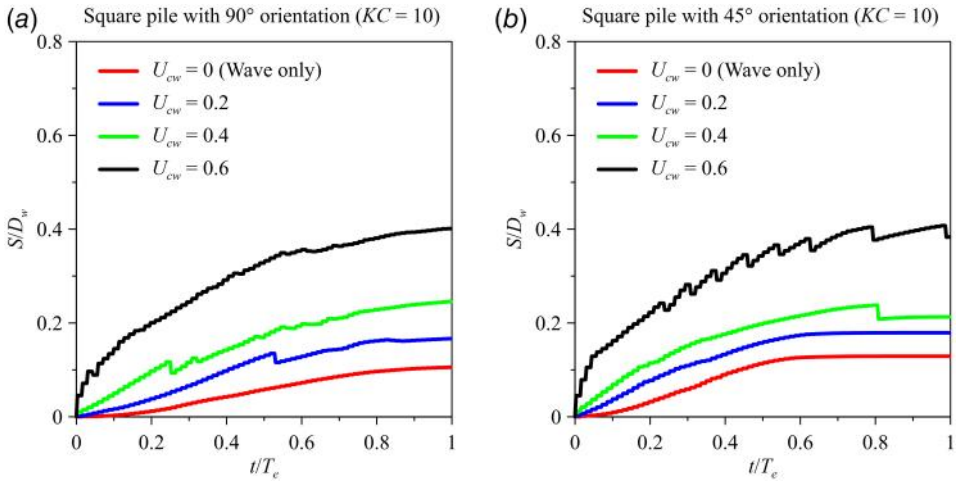

Fig. 19 Temporal change in S/D_w at square pile with (*a*) 90 deg and (*b*) 45 deg orientations for KC = 10

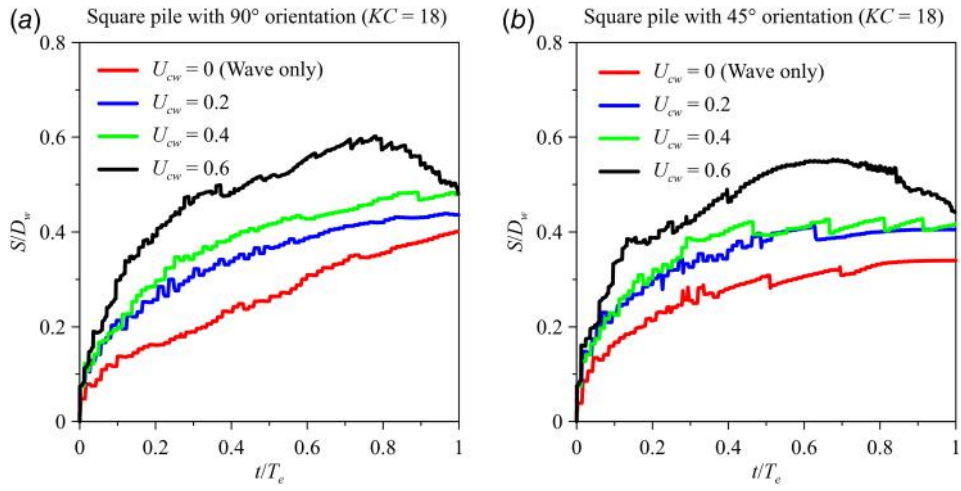

Fig. 20 Temporal change in S/D_w at square pile with (*a*) 90 deg and (*b*) 45 deg orientations for KC = 18

$$S/D_w = 0.185 \times \ln(\mathrm{Fr}_a) + 0.520 \quad (0.075 < \mathrm{Fr_a} < 0.772,\ \ 3.9 < KC < 18) \tag{16}$$

Figure 23 compares the equilibrium scour depth normalized by pile width (S/D_w) obtained from the present numerical simulations for a square pile under wave-only conditions with the empirical formulations proposed by Sumer and Fredsøe [76]. The results are shown for two pile orientations such as 45 deg and 90 deg with respect to the wave direction. For both orientations, the normalized scour depth increases with the KC number, indicating the growing influence of flow reversal and vortex shedding at higher KC values. The present CFD results for the square pile show good qualitative agreement with the empirical trends of Sumer and Fredsøe (2002), though slight deviations are observed due to the difference in pile orientation. At lower KC values (3.9 and 5.75), the scour depths remain

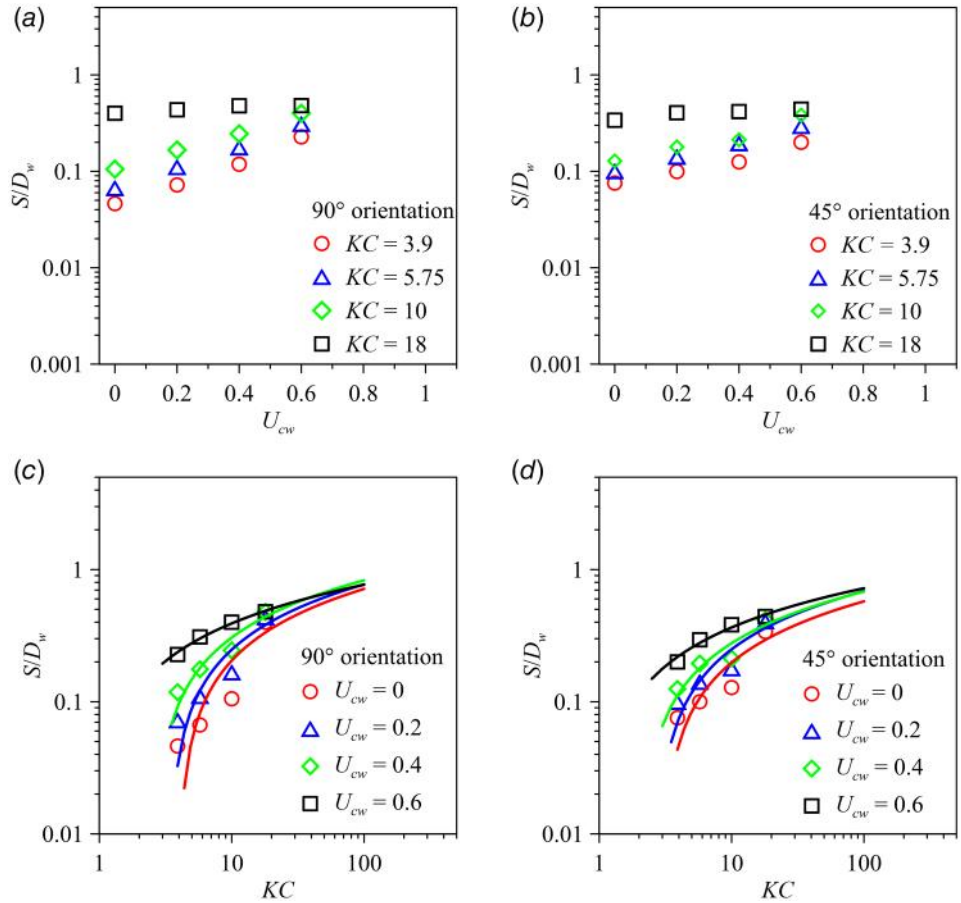

Fig. 21 Variation of S/D_w with U_{cw} for square pile for (*a*) 90 deg and (*b*) 45 deg orientation. Variation of S/D_w with KC number for square pile for (*c*) 90 deg and (*d*) 45 deg orientation.

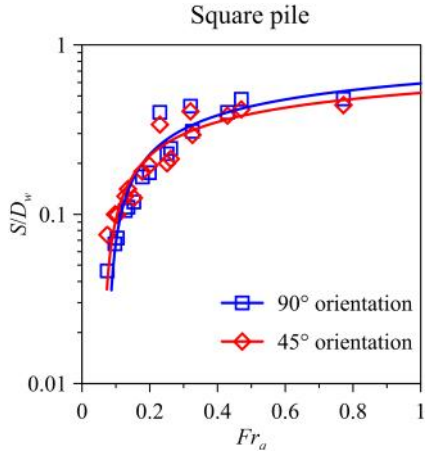

Fig. 22 The variation of S/D_w versus Fr_a for both orientations of the square pile

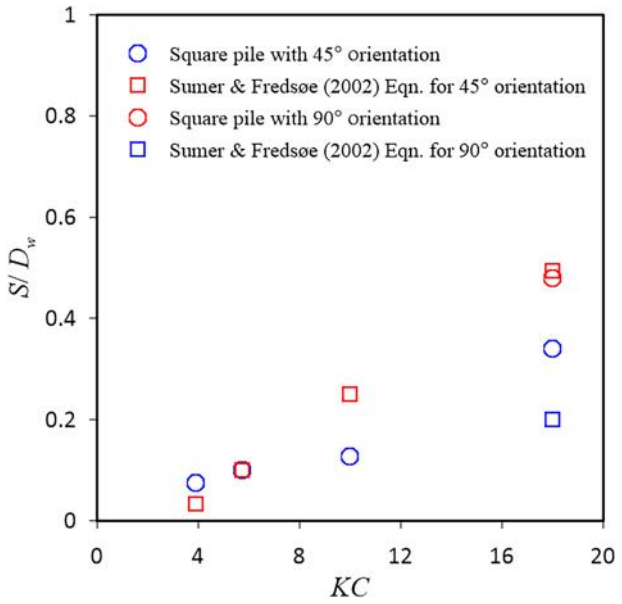

Fig. 23 Comparison of normalized equilibrium scour depth (S/D_w) with KC number for square piles under the wave-only condition. Results from the present study are shown for 45 deg and 90 deg pile orientations and compared with the empirical equations of Sumer and Fredsøe [76].

relatively small, while for KC numbers greater than or equal to 10, scour depth increases more rapidly, particularly for the 90 deg orientation. The scour depth at 45 deg orientation is consistently lower than that at 90 deg, suggesting that flow separation and vortex intensity are reduced when the pile face is inclined to the incoming wave.

4 Conclusions

This study investigates the scour phenomenon around square piles placed at 45 deg and 90 deg angles using a three-dimensional CFD model with the LSM technique. Careful analysis of the numerical results led to the following main conclusions:

- For low KC numbers ($KC < 10$), larger scour depths are observed around square piles oriented at 45 deg compared to 90 deg. This is primarily due to vortex shedding, which begins at $KC \geq 4$ for 45 deg orientations and $KC \geq 11$ for 90 deg orientations. However, at a larger KC number ($KC = 18$), the larger depths are observed around square piles oriented at 90 deg compared to 45 deg. This is mainly due to wave-induced forces domination at 90 deg orientation, which causes greater flow separation and turbulence around the pile, leading to intensified scour compared to the streamlined 45 deg orientation.
- The wave–current parameter (U_{cw}) strongly affects the scour depth (S/D_w) around both orientations, when the KC number is low ($KC \leq 10$). Scour depth increases gradually as U_{cw} increases from 0 to 0.4 and then rises rapidly. However, at higher KC numbers ($KC = 18$), the influence of U_{cw} becomes negligible due to the dominant role of wave-induced forces in the scour process.
- S/D_w values of the square pile oriented at 45 deg are greater than those of the square pile oriented at 90 deg for $U_{cw} \leq 0.2$. However, the S/D_w values of the square pile oriented at 90 deg become greater than those of the square pile of orientation 45 deg for $U_{cw} > 0.2$. This may mainly be due to the formation of asymmetric flow separation and stronger vortex shedding around the square pile oriented at 45 deg for $U_{cw} \leq 0.2$.
- S/D_w values show a good correlation with the Fr_a for a wide range of KC ($3.9 < KC < 18$). As the Fr_a increases to 1.0, the S/D_w value approaches an asymptotic value of 0.6 for 90 deg oriented square pile and 0.5 for 45 deg oriented square pile. This difference arises because the 90 deg orientation generates stronger vortices, compared to the 45 deg orientation.

These findings provide several insights relevant to coastal and offshore engineering practice. The results indicate that pile orientation significantly influences local scour formation in combined wave–current environments. For sites characterized by low KC numbers or weak to moderate currents, orienting square piles at 45 deg to the flow may reduce local scour and enhance foundation stability. However, under high KC regimes or strong current–wave interaction, piles oriented perpendicular to the flow (90 deg) are likely to experience greater scour and thus require enhanced protection measures such as collars, rock armoring, or scour mats. The results also emphasize the importance of considering the combined effect of waves and currents rather than treating them independently during the design and assessment of pile-supported coastal and offshore structures. Incorporating these hydrodynamic interactions in design guidelines can improve the prediction accuracy of scour depth and lead to safer and more cost-effective foundation solutions.

5 Possible Future Research Directions

The present study provides detailed insights into the scour mechanisms around square piles with 45 deg and 90 deg orientations in combined wave–current environments using a validated three-dimensional CFD model. Nevertheless, several avenues remain open for future research to further advance the understanding of scour around coastal and offshore structures.

Future investigations could explore the influence of different pile cross-sections, such as rectangular or elliptical cross-sections, as well as pile group configurations, to better understand how shape-induced flow separation and vortex interactions influence scour formation. The effect of sediment characteristics also deserves further attention, as the current work considered uniform, noncohesive sediment, whereas cohesive or mixed sediments could provide more realistic insights applicable to natural seabeds where composition varies.

In addition, extending the analysis to irregular, oblique, or multidirectional wave–current interactions would enhance the applicability of the findings to real coastal environments. Studies incorporating variations in wave height, spectral wave distributions, and turbulence intensities could also yield a more

comprehensive understanding of scour evolution. Additionally, investigating scale effects through controlled laboratory testing and field-scale validation would help establish greater confidence in the numerical model's predictive capabilities for prototype structures such as bridge piers, offshore wind foundations, and harbor piles. Finally, the inclusion and evaluation of scour countermeasures, such as collars, riprap, or artificial mats, under combined wave–current flows could provide valuable design guidance for coastal engineers.

Acknowledgment

This study is a component of a university strategic initiative titled "Computational Fluid Dynamics Modeling of Hydrodynamics and Scour Around Coastal Structures," supported by the Science and Engineering Research Board (SERB), Department of Science and Technology (DST), India, under Grant No. CRG/2022/002353. Additionally, the investigation benefited from the super-computing facility of IIT Kharagpur.

Conflict of Interest

There are no conflicts of interest.

Data Availability Statement

The datasets generated and supporting the findings of this article are obtainable from the corresponding author upon reasonable request.

References

[1] Afzal, M. S., and Kumar, L., 2021, "Propagation of Waves Over a Rugged Topography," J. Ocean Eng. Sci., **7**(1), pp. 14–28.
[2] Afzal, M. S., Holmedal, L. E., and Myrhaug, D., 2021, "Sediment Transport in Combined Wave and Current Seabed Boundary Layers Due to Streaming," J. Hydraul. Eng., **147**(4), p. 4021007.
[3] Vanhellemont, Q., and Ruddick, K., 2014, "Turbid Wakes Associated With Offshore Wind Turbines Observed With Landsat 8," Remote Sens. Environ., **145**, pp. 105–115.
[4] Alhaddad, S., and Elerian, M., 2024, "Mitigating Suspended-Sediment Environmental Pressure in Subsea Engineering Through Colliding Turbidity Currents," Results Eng., **21**(Jan.), p. 101916.
[5] Alhaddad, S., de Wit, L., Labeur, R. J., and Uijttewaal, W., 2020, "Modeling of Breaching-Generated Turbidity Currents Using Large Eddy Simulation," J. Mar. Sci. Eng., **8**(9), p. 728.
[6] Alhaddad, S., Labeur, R. J., and Uijttewaal, W., 2020, "Large-Scale Experiments on Breaching Flow Slides and the Associated Turbidity Current," J. Geophys. Res. Earth Surf., **125**(10), p. e2020JF005582.
[7] Alhaddad, S., Weij, D., van Rhee, C., and Keetels, G., 2023, "Stabilizing and Destabilizing Breaching Flow Slides," J. Mar. Sci. Eng., **11**(3), p. 560.
[8] Chiew, Y.-M., and Melville, B. W., 1987, "Local Scour Around Bridge Piers," J. Hydraul. Res., **25**(1), pp. 15–26.
[9] Dey, S., 1995, "Three-Dimensional Vortex Flow Field Around a Circular Cylinder in a Quasi-equilibrium Scour Hole," Sadhana, **20**(6), pp. 871–885.
[10] Afzal, M. S., Bihs, H., Kamath, A., and Arntsen, Ø. A., 2015, "Three-Dimensional Numerical Modeling of Pier Scour Under Current and Waves Using Level-Set Method," ASME J. Offshore Mech. Arct. Eng., **137**(3), p. 032001.
[11] Kobayashi, T., 1992, "3D Analysis of Flow Around a Vertical Cylinder on a Scoured Bed," Coast. Eng., **1**(23), pp. 3482–3495.
[12] Kobayashi, T., and Oda, K., 1994, "Experimental Study on Developing Process of Local Scour Around a Vertical Cylinder," Coast. Eng., **1**(24), pp. 1284–1297.
[13] Link, O., Castillo, C., Pizarro, A., Rojas, A., Ettmer, B., Escauriaza, C., and Manfreda, S., 2017, "A Model of Bridge Pier Scour During Flood Waves," J. Hydraul. Res., **55**(3), pp. 310–323.
[14] Melville, B. W., and Chiew, Y.-M., 1999, "Time Scale for Local Scour at Bridge Piers," J. Hydraul. Eng., **125**(1), pp. 59–65.
[15] Melville, B. W., and Coleman, S. E., 2000, *Bridge Scour*, Water Resources Publication, United States of America.
[16] Prepernau, U., Grüne, J., Sparboom, U., Schmidt-Koppenhagen, R., Wang, Z., and Oumeraci, H., 2009, "Large-Scale Model Study on Scour Around Slender Monopiles Induced by Irregular Waves," *Coastal Engineering 2008: (In 5 Volumes)*, Hamburg, Germany.
[17] Zanke, U. C. E., Hsu, T.-W., Roland, A., Link, O., and Diab, R., 2011, "Equilibrium Scour Depths Around Piles in Noncohesive Sediments Under Currents and Waves," Coast. Eng., **58**(10), pp. 986–991.
[18] Khosronejad, A., Kang, S., and Sotiropoulos, F., 2012, "Experimental and Computational Investigation of Local Scour Around Bridge Piers," Adv. Water Resour., **37**, pp. 73–85.
[19] Chen, B., and Li, S., 2018, "Experimental Study of Local Scour Around a Vertical Cylinder Under Wave-Only and Combined Wave-Current Conditions in a Large-Scale Flume," J. Hydraul. Eng., **144**(9), p. 4018058.
[20] Lyu, X., Cheng, Y., Wang, W., An, H., and Li, Y., 2021, "Experimental Study on Local Scour Around Submerged Monopile Under Combined Waves and Current," Ocean Eng., **240**, p. 109929.
[21] Qi, W.-G., and Gao, F.-P., 2014, "Physical Modeling of Local Scour Development Around a Large-Diameter Monopile in Combined Waves and Current," Coast. Eng., **83**, pp. 72–81.
[22] Qi, W., and Gao, F., 2014, "Equilibrium Scour Depth at Offshore Monopile Foundation in Combined Waves and Current," Sci. China Technol. Sci., **57**(5), pp. 1030–1039.
[23] Sumer, B. M., and Fredsøe, J., 2001, "Scour Around Pile in Combined Waves and Current," J. Hydraul. Eng., **127**(5), pp. 403–411.
[24] Sumer, B. M., Petersen, T. U., Locatelli, L., Fredsøe, J., Musumeci, R. E., and Foti, E., 2013, "Backfilling of a Scour Hole Around a Pile in Waves and Current," J. Waterw. Port Coastal Ocean Eng., **139**(1), pp. 9–23.
[25] Dey, S., 2014, *Fluvial Hydrodynamics*, Springer, New York.
[26] Kumar, L., and Afzal, M. S., 2022, "A Review of the State of Research on Bridge Pier Scour Under Combined Action of Waves and Current," Acta Geophys., **71**(5), pp. 2359–2379.
[27] Kumar, L., and Afzal, M. S., 2023, "Experimental and Numerical Modelling of Scour at Vertical Wall Abutment Under Combined Wave-Current Flow in Low KC Regime," Ocean Eng., **285**(P2), p. 115394.
[28] Sumer, B., Fredsøe, J., and Christiansen, N., 1992, "Scour Around Vertical Pile in Waves," J. Waterw. Port Coastal Ocean Eng., **118**(1), pp. 15–31.
[29] Sumer, B., Christiansen, N., and Fredsøe, J., 1993, "Influence of Cross Section on Wave Scour Around Piles," J. Waterw. Port Coastal Ocean Eng., **119**(5), pp. 477–495.
[30] Kumar, L., and Afzal, M. S., 2023, "Estimating Pier Scour Depth Under Combined Waves and Current Using Boosting Machine-Learning Models," Acta Geophys., **72**(3), pp. 1895–1911.
[31] Sumer, B. M., Christiansen, N., and Fredsøe, J., 1997, "The Horseshoe Vortex and Vortex Shedding Around a Vertical Wall-Mounted Cylinder Exposed to Waves," J. Fluid Mech., **332**, pp. 41–70.
[32] Soulsby, R. L., and Whitehouse, R. J. S., 1997, "Threshold of Sediment Motion in Coastal Environments," Pacific Coasts and Ports' 97: Proceedings of the 13th Australasian Coastal and Ocean Engineering Conference and the 6th Australasian Port and Harbour Conference, Wallingford, UK.
[33] Umeyama, M., 2005, "Reynolds Stresses and Velocity Distributions in a Wave-Current Coexisting Environment," J. Waterw. Port Coastal Ocean Eng., **131**(5), pp. 203–212.
[34] Umeyama, M., 2009, "Changes in Turbulent Flow Structure Under Combined Wave-Current Motions," J. Waterw. Port Coastal Ocean Eng., **135**(5), pp. 213–227.
[35] Umeyama, M., 2011, "Coupled PIV and PTV Measurements of Particle Velocities and Trajectories for Surface Waves Following a Steady Current," J. Waterw. Port Coastal Ocean Eng., **137**(2), pp. 85–94.
[36] Schendel, A., Welzel, M., Schlurmann, T., and Hsu, T.-W., 2020, "Scour Around a Monopile Induced by Directionally Spread Irregular Waves in Combination With Oblique Currents," Coast. Eng., **161**, p. 103751.
[37] Dutta, D., Bihs, H., and Afzal, M. S., 2022, "Computational Fluid Dynamics Modelling of Hydrodynamic Characteristics of Oscillatory Flow Past a Square Cylinder Using the Level Set Method," Ocean Eng., **253**, p. 111211.
[38] Dutta, D., Afzal, M. S., and Alhaddad, S., 2023, "3D CFD Study of Scour in Combined Wave and Current Flows Around Rectangular Piles With Varying Aspect Ratios," Water, **15**(8), p. 1541.
[39] Gautam, S., Dutta, D., Bihs, H., and Afzal, M. S., 2021, "Three-Dimensional Computational Fluid Dynamics Modelling of Scour Around a Single Pile Due to Combined Action of the Waves and Current Using Level-Set Method," Coast. Eng., **170**, p. 104002.
[40] Quezada, M., Tamburrino, A., and Niño, Y., 2019, "Numerical Study of the Hydrodynamics of Waves and Currents and Their Effects in Pier Scouring," Water, **11**(11), p. 2256.
[41] Kumar, L., and Afzal, M. S., 2023, "Numerical Simulations of Scour Around Vertical Wall Abutments With Varying Aspect Ratios Under Combined Waves and Current Flows," J. Mar. Sci. Eng., **11**(10), p. 1886.
[42] Ahmad, N., Bihs, H., Myrhaug, D., Kamath, A., and Arntsen, Ø. A., 2018, "Three-Dimensional Numerical Modelling of Wave-Induced Scour Around Piles in a Side-by-Side Arrangement," Coast. Eng., **138**, pp. 132–151.
[43] Bihs, H., and Olsen, N., 2011, "Numerical Modeling of Abutment Scour With the Focus on the Incipient Motion on Sloping Beds," J. Hydraul. Eng., **137**(10), pp. 1287–1292.
[44] Bihs, H., and Olsen, N. R. B., 2008, "Three Dimensional Numerical Modeling of Pier Scour," Fourth International Conference on Scour and Erosion, ICSE 4, Tokyo, Japan, Nov. 5.
[45] Bihs, H., Kamath, A., Chella, M. A., Aggarwal, A., and Arntsen, Ø. A., 2016, "A New Level Set Numerical Wave Tank With Improved Density Interpolation for Complex Wave Hydrodynamics," Comput. Fluids, **140**, pp. 191–208.
[46] Kumar, L., Afzal, M. S., and Alhaddad, S., 2024, "Computational Investigation of Scour Around Submerged Square Piles in Wave-Current Flows," Ocean Eng., **314**(P2), p. 119766.
[47] Kumar, L., and Afzal, M. S., 2024, "Computational Fluid Dynamics Modeling of Scour Around Abutment Geometries Under Combined Effects of Waves and Currents," Ocean Eng., **294**(Jan.), p. 116812.

[48] Ahmad, N., Bihs, H., Myrhaug, D., Kamath, A., and Arntsen, Ø. A., 2019, "Numerical Modelling of Pipeline Scour Under the Combined Action of Waves and Current With Free-Surface Capturing," Coast. Eng., **148**, p. 19–35.
[49] Jiang, G. S., and Shu, C. W., 1996, "Efficient Implementation of Weighted ENO Schemes," J. Comput. Phys., **126**(1), pp. 202–228.
[50] Jiang, G. S., and Peng, D., 2000, "Weighted ENO Schemes for Hamilton Jacobi Equations," SIAM J. Sci. Comput., **21**(6), pp. 2126–2143.
[51] Chorin, A. J., 1968, "Numerical Solution of the Navier-Stokes Equation," Math. Comput., **22**(104), pp. 745–762.
[52] Gottlieb, S., and Shu, C.-W., 1998, "Total Variation Diminishing Runge-Kutta Schemes," Math. Comput., **67**(221), pp. 73–85.
[53] Griebel, M., Dornseifer, T., and Neunhoeffer, T., 1998, *Numerical Simulation in Fluid Dynamics, a Practical Introduction*, SIAM, Philadelphia, PA.
[54] Wilcox, D. C., 1994, "Simulation of Transition With a Two-Equation Turbulence Model," AIAA J., **32**(2), pp. 247–255.
[55] Kraft, S., Wang, Y., and Oberlack, M., 2011, "Large Eddy Simulation of Sediment Deformation in a Turbulent Flow by Means of Level-Set Method," J. Hydraul. Eng., **137**(11), pp. 1394–1405.
[56] Shields, A., 1936, "Anwendung der Aehnlichkeitsmechanik und der Turbulenzforschung auf die Geschiebebewegung," Mitteilungen der Preussischen Versuchsanstalt fur Wasserbau und Schiffbau, **26**(5), pp. 1–5.
[57] Dey, S., 2001, "Experimental Studies on Incipient Motion of Sediment Particles on Generalized Sloping Fluvial Beds," J. Sediment Res., **16**(3), pp. 391–398.
[58] Ikeda, S., 1982, "Incipient Motion of Sand Particles on Side Slopes," J. Hydraul. Div. ASCE, **108**(1), pp. 95–114.
[59] Lane, E. W., 1955, "Design of Stable Channels," Trans. ASCE, **120**(1), pp. 1234–1260.
[60] Kovacs, A., and Parker, G., 1994, "A New Vectorial Bedload Formulation and Its Application to the Time Evolution of Straight River Channels," J. Fluid Mech., **267**, pp. 153–183.
[61] Dey, S., 2003, "Threshold of Sediment Motion on Combined Transverse and Longitudinal Sloping Beds," J. Hydraul. Res., **41**(4), pp. 405–415.
[62] Burkow, M., and Griebel, M., 2016, "A Full Three Dimensional Numerical Simulation of the Sediment Transport and the Scouring at a Rectangular Obstacle," Comput. Fluids, **125**, pp. 1–10.
[63] Roulund, A., Sumer, B. M., Fredsøe, J., and Michelsen, J., 2005, "Numerical and Experimental Investigation of Flow and Scour Around a Circular Pier," J. Fluid Mech., **534**, pp. 351–401.
[64] van Rijn, L. C., 1984, "Sediment Transport, Part I: Bed Load Transport," J. Hydraul. Eng., **110**(10), pp. 1431–1457.
[65] van Rijn, L. C., 1984, "Sediment Transport, Part II: Suspended Load Transport," J. Hydraul. Eng., **110**(11), pp. 1613–1641.
[66] Hunt, J. N., 1954, "The Turbulent Transport of Suspended Sediment in Open Channels," Proc. R. Soc. Lond. A Math. Phys. Sci., **224**(1158), pp. 322–335.
[67] Afzal, M. S., Bihs, H., and Kumar, L., 2020, "Computational Fluid Dynamics Modeling of Abutment Scour Under Steady Current Using the Level Set Method," Int. J. Sediment Res., **35**(4), pp. 355–364.
[68] Jacobsen, N. G., Fuhrman, D. R., and Fredsøe, J., 2011, "A Wave Generation Toolbox for the Open-Source CFD Library: OpenFOAM," Int. J. Numer. Methods Fluids, **70**(9), pp. 1073–1088.
[69] Bihs, H., and Kamath, A., 2017, "A Combined Level Set/Ghost Cell Immersed Boundary Representation for Floating Body Simulations," Int. J. Numer. Methods Fluids, **83**(12), pp. 905–916.
[70] Xiao, Y., Jia, H., Guan, D., Liang, D., Yuan, S., and Tang, H., 2021, "Experimental Investigation on Scour Topography Around High-Rise Structure Foundations," Int. J. Sediment Res., **36**(3), pp. 348–361.
[71] Cheng, H., Cheng, Y., Wang, X., Xia, B., Lyu, X., Zheng, Y., and Zhang, J., 2022, "Experimental Study of Local Scour Around Inclined Piles in Combined Waves and Current," Ocean Eng., **266**, p. 112511.
[72] Bordbar, A., Sharifi, S., and Hemida, H., 2021, "Investigation of the Flow Behaviour and Local Scour Around Single Square-Shaped Cylinders at Different Positions in Live-Bed," Ocean Eng., **238**, p. 109772.
[73] Bihs, H., 2011, *Three-Dimensional Numerical Modeling of Local Scouring in Open Channel Flow*, NTNU Trondheim, Norway.
[74] Williamson, C. H. K., 1985, "Evolution of a Single Wake Behind a Pair of Bluff Bodies," J. Fluid Mech., **159**, pp. 1–18.
[75] Zhao, M., Cheng, L., and Zang, Z., 2010, "Experimental and Numerical Investigation of Local Scour Around a Submerged Vertical Circular Cylinder in Steady Currents," Coast. Eng., **57**(8), pp. 709–721.
[76] Sumer, B., and Fredsøe, J., 2002, *The Mechanics of Scour in the Marine Environment*, World Scientific, Singapore.